SLAC-PUB-10494
June 2004

X-ray production by cascading stages of a High-Gain Harmonic Generation Free-Electron Laser I: basic theory*

Juhao Wu†
Stanford Linear Accelerator Center, Stanford University, Stanford, CA 94309

Li Hua Yu
National Synchrotron Light Source, Brookhaven National Laboratory, Upton, NY 11973

We study a new approach to produce x-ray by cascading several stages of a High-Gain Harmonic Generation (HGHG) Free-Electron Laser (FEL). Besides the merits of a Self-Amplified Spontaneous Emission (SASE) scheme, an HGHG scheme could also provide much better stability of the radiation power, controllable short pulse length, more stable central wavelength, and radiation with better longitudinal coherence. Detailed design and optimization scheme, simulation results and analytical estimate formulae are presented. To lay results on a realistic basis, the electron bunch parameters used in this paper are restricted to be those of DESY TTF and SLAC LCLS projects; however, such sets of parameters are not necessary to be optimized for an HGHG FEL.

Submitted to Physical Review E

PACS numbers: 41.60.Cr, 42.25.Kb; 42.55.Vc; 42.65.Ky

I. INTRODUCTION

Short wavelength Free-Electron Lasers (FELs) are perceived as the next generation of synchrotron light sources. In the past decade, significant advances have been made in the theory and technology of high-brightness electron beams and single-pass FELs. These developments facilitate the construction of practical vacuum ultraviolet (VUV) FELs and make x-ray FELs possible. Self-Amplified Spontaneous Emission (SASE) [1–15] and High-Gain Harmonic Generation (HGHG) [16–24] are the two leading candidates for VUV and x-ray FELs. The first HGHG proof-of-principle experiment [19, 20] succeeded in August, 1999 in Brookhaven National Laboratory. The experimental results agree with the theory prediction. The following advantages of the HGHG FEL over the SASE FEL were confirmed: 1. much better longitudinal coherence, 2. much narrower bandwidth, 3. more stable central wavelength. These HGHG FEL advantages were further confirmed recently in ultraviolet wavelength regime [23, 24]. These stimulated our interest in investigating whether it is now feasible to produce an x-ray FEL by the HGHG-based scheme. This is the purpose of this study.

In this paper, we first describe the principle of HGHG FEL in Section II. Then in Section III, we give the details of how to produce x-ray by the HGHG scheme. The stability of such an HGHG scheme and its sensitivity to electron quality are discussed in Section IV. The results are presented in Section V. Finally, in Section VI, after some discussion, we present our conclusions.

II. THE HGHG PRINCIPLE

The HGHG scheme was inspired by some earlier and related ideas [25–37]. A one-stage HGHG FEL scheme has three components: one undulator used as the modulator, one dispersion section, and a second undulator used as the radiator. As shown in Fig. 1, a seed laser, together with an electron beam, is introduced into the modulator. In the modulator, the seed laser (λ=10.6 μm) interacts with the e-beam, and a small energy modulation is formed in the e-beam. Note that the energy modulation is induced by a high-peak-power, high quality seed laser, rather than by the spontaneous emission of the electron beam itself. The energy-modulated e-beam passes through the dispersion section (a three-dipole chicane), where the energy modulation in the e-beam is converted into spatial modulation. Again, because the high-peak-power, high quality seed laser dominates the spontaneous emission from the electron beam itself, the phase information of the seed laser is preserved in the spatial modulation in the electron beam. Abundant harmonics exist in such spatially modulated e-beam, which then enters the radiator. The radiator is designed to be resonant to one of the harmonics of the seed laser frequency ω. Once the spatially modulated e-beam enters the radiator, rapid coherent emission at this resonant harmonic n ω is produced, and then this harmonic is further amplified exponentially until saturation. This is exactly the main set-up for the first HGHG experiment [19, 20]. In this experiment, the input CO_2 seed laser power was 0.7 MW at 10.6 μm, the output HGHG FEL power was about 35 MW at 5.3 μm. Compared with the seed laser, Harmonic Generation was achieved, i.e. the second harmonic was radiated. This harmonic is then amplified by a High

*Work supported by Department of Energy contract DE–AC03–76SF00515 (Juhao Wu) and contract DE–AC02–98CH10886 (Juhao Wu and Li Hua Yu).
†Electronic address: jhwu@SLAC.Stanford.EDU

Gain FEL process. The final HGHG FEL pulse energy was measured to be $\sim 10^7$ times as large as the spontaneous radiation and $\sim 10^6$ times as large as the SASE FEL. This experiment proved the principle of the HGHG FEL, and also demonstrated the advantages of HGHG FEL.

In order to distinguish the relative local energy spread before the e-beam enters the undulator from the relative local energy spread growth due to the quantum diffusion effect [38] when the e-beam traverses the undulator, in our paper we use "initial relative local energy spread" to refer to the value before the e-beam enters the undulator. Thus in Fig. 1, $\sigma_\gamma/\gamma = 0.043\%$ is the initial relative local energy spread.

III. THE HGHG SCHEME TO PRODUCE X-RAY

A. Design scheme

We now describe the approach to generate x-ray by cascading HGHG stages [39, 40]. Cascading two stages of HGHG for soft x-ray FEL has been proposed before [41, 42]. To reach x-ray, we need more than two stages and there are new issues to be addressed here.

Lasers with wavelengths of thousands Ångstrom are commercially available. We hoped to produce x-rays of only several Ångstroms. To achieve 1 Å by one step of HGHG would require extremely high harmonics, of the order of several thousands. Previous studies [41, 42] tried to reach XUV wavelengths by one stage of Harmonic Generation followed by an amplifier Such an approach requires very high input seed laser power to get high harmonic output. Beyond the 60th harmonic, this becomes difficult. Also, as we will discuss in the Sec. IV, trying to reach a very high harmonic of the seed laser causes the stability of the output FEL to be bad. Hence, we need to cascade several stages of HGHG, and there are new isses to be addressed. We make the following modifications.

1. We need multiple stages. During each stage the nth harmonic of the seed laser will be produced at the end of the radiator, and then this harmonic will be used as the seed for the next stage. In reality, n could not be too large. In our design we use $n = 3$, 4 and 5 to achieve stable performance. If we begin with a commercial laser of thousands of Ångstrom as the seed, we need several stages to get down to the hard x-rays with a wavelength of several Ångstroms.

2. Conceptually, the device is composed of two parts, a converter [28], and an amplifier. The converter, consisting of several stages, converts the seed laser to the designed wavelength step by step. Then at the end, an amplifier exponentially amplifies the radiation obtained from the last stage to saturation.

3. Except for the first two stages and the last amplifier, each stage only converts the light to its nth harmonics. Exponential growth is not required as long as the harmonic power is high enough to be used as the seed for the next stage.

4. Since the energy of the electron beam should match the corresponding radiation wavelength to achieve best efficiency, electron beam will have different optimized energy for each stage. For the purpose of comparison, we restrict ourselves to the parameters from the DESY TTF, and SLAC LCLS projects. The one with the lower energy, $E = 2$ GeV, works in the longer-wavelength stages, and the other, $E = 14$ GeV, works in the shorter-wave length stages. Without this restriction, further optimization of the results presented in this paper should be possible [43].

5. As we will illustrate in the following, the phase mixing induced by the emittance in the dispersion section is negligible compared with that induced by the local energy spread. Because of the Natural Emittance Effect Reduction (NEER) mechanism, the emittance will play a less important role in the converter, i.e., the Harmonic Generation stages. For the purpose of comparison with the SASE FEL, in this paper we restrict ourselves to the parameters from DESY TTF with normalized emittance $\epsilon_n = 2\,\pi$ mm-mrad, and SLAC LCLS project with normalized emittance $\epsilon_n = 1.5\,\pi$ mm-mrad. A new operation mode by optimizing the electron beam parameters in a different way is underinvestigation [43].

6. Since we need cascade several stages of HGHG, we need some extra components. Each stage will be the same as that shown in Fig. 1, i.e., each stage will consist of one modulator, a dispersion section, and one radiator. The physics process in each stage will be the same as in the recent experiment [19, 20]. During the process, the output radiation has disturbed a part of the e-beam, which coincides with it. Therefore, to achieve the best efficiency in the next stage of HGHG, we need use a fresh e-beam. There are two methods for this. The first is to shift the laser (i.e., the output radiation from the previous HGHG stage) to the front part of the same e-beam, so that the laser will interact with a "fresh" part of the same e-beam. The second is to introduce a different electron bunch for each stage, so that again the laser will interact with a "fresh" bunch. This is the "fresh bunch technique" [44]. Both are schematically plotted in Fig. 2. For the first case, i.e. using the same e-beam, we use a "shifter" to "shift" the laser to the "fresh" part of the same e-beam.

Let us now present the details of the whole device. As shown in Fig. 3, we consider an available laser with a wavelength of $2,250$ Å, and a peak power of $P_{in} = 1$ GW. The corresponding start-up shot-noise power [10] is only about $P_{noise} \approx 60$ W. Thus the input seed laser power dominates the shot-noise power. This is true for all seed lasers into the five stages and the last amplifier. This dominance is necessary, because even though there is only negligible noise power in the initial stage, the signal-to-noise ratio of the final radiation at 1.5 Å might be degraded [45]. Calculation [43] shows that a 1 GW seed laser could ensure that the signal-to-noise ratio at

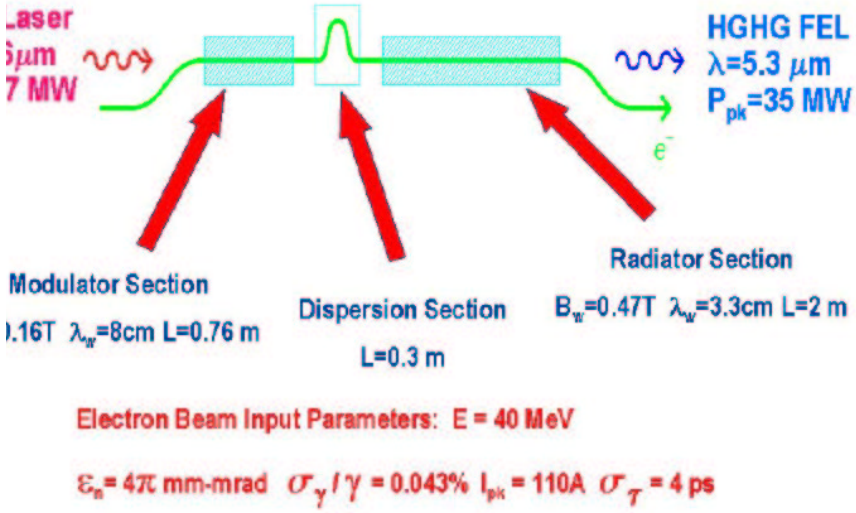

FIG. 1: Schematic plot of the set-up of the first lasing HGHG experiment.

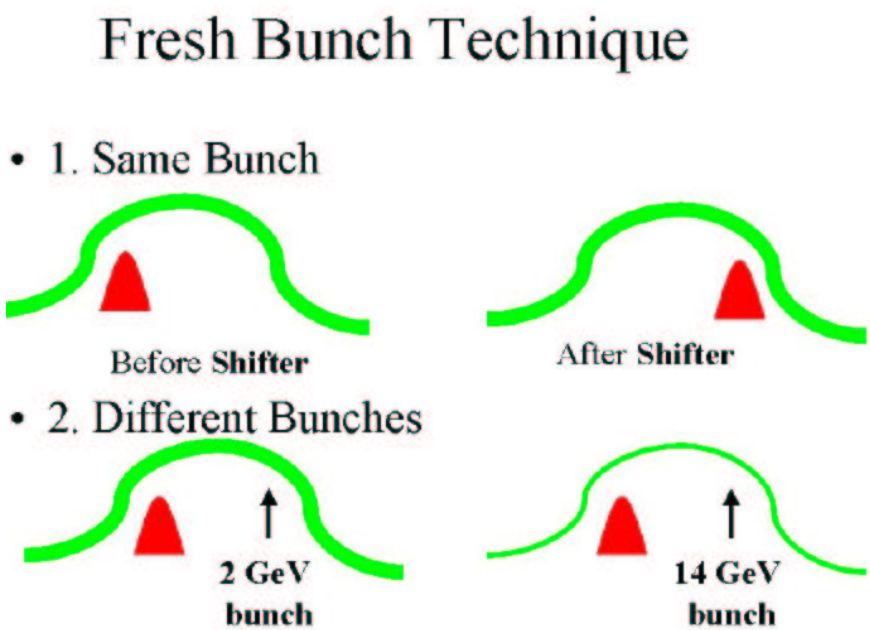

FIG. 2: Schematic plot of the two types of the "fresh bunch technique". In the first case, we use the same e-beam; in the second case, the first e-beam is dumped and a second e-beam is introduced. The filled pulse stands for the laser pulse.

the final 1.5 Å radiation to be around 10. After 5 stages, we get 1.5 Å radiation, and then this 1.5 Å radiation is amplified to the saturation region with a peak power around 15 GW by traversing the last undulator, called the amplifier. The parameters for the electron beam, the undulators, and the dispersion section are given in the table of Fig. 3. Let us first explain the meaning of each parameter in Fig. 3. The number in the first row stands for the output power of each stage. The output power of one stage is the input power of the next stage, though diffraction effect should be taken into consideration as we will discuss shortly. The second row stands for the corresponding wavelength of the radiation. The e-beam parameters are printed just below the schematic device. The relative local energy spread given in the plot is the initial relative local energy spread before the e-beam goes into the first modulator. This is increased by spontaneous radiation. We take this into account [38], and give its value at the end of the modulators in the table. For the first two stages, where the wavelength of the radiation is comparably long, we use a lower-energy e-beam. The parameters are those of the DESY TTF, except that the energy is 2 GeV. The e-beam has a peak current of $2,500$ Amp, an energy of 2 GeV, a normalized emittance $\epsilon_n = 2\,\pi$ mm-mrad and an initial relative local energy spread $\frac{\sigma_\gamma}{\gamma} = 5 \times 10^{-4}$. For the following stages, a higher energy e-beam is used. It has the parameters of those of SLAC LCLS project. That e-beam has a peak current of $3,400$ Amp, an energy of 14 GeV, normalized emittance $\epsilon_n = 1.5\,\pi$ mm-mrad and an initial relative local energy spread $\frac{\sigma_\gamma}{\gamma} = 6 \times 10^{-5}$. In the table, the fist row gives the radiation wavelength; the second row, the undulator period, and the third row the dispersion strength. The fourth row gives the relative local energy spread (with the quantum diffusion effect [38] taken into account) at the end of the modulator in each stage. This number is used as the effective relative local energy spread in the calculation for this paper. We further upgrade [46] our code to simulate the growing of the relative local energy spread along the undulator, and the results obtained using this effective relative local energy spread agree well with the results given by the upgraded code. The fifth row gives the length of the undulators (modulators, radiators, and the amplifier). For example, the last amplifier has a length of 33.5 m. The sixth row gives the power e-folding length in each undulator without energy modulation. The table has six boxes; the first five boxes stand for the five stages and the last one for the amplifier. In each of the five boxes, which stand for each stage, the left column gives the parameters for the modulator and the right column those for the radiator; the numbers in the middle stand for the dispersion strength $\frac{d\psi}{d\gamma}$ and the relative local energy spread $\frac{\sigma_\gamma}{\gamma}$ at the end of the modulator. For example, the second box stands for the second stage. The left column in this second box stands for the modulator of the second stage. The table shows that in the modulator the resonant radiation has a wavelength of 450 Å, the modulator has a period of 4.6 cm, the length of the modulator is 0.7 m, and the corresponding power e-folding length without energy modulation is 0.6 m. The right column shows that the radiation in the radiator has a wavelength of 90 Å, the radiator has a period of 3.2 cm, the length of the radiator is 4 m, and the corresponding power e-folding length is 0.7 m. In the middle, i.e. 0.21, stands for the dispersion strength $\frac{d\psi}{d\gamma}$, and 5×10^{-4} stands for the relative local energy spread $\frac{\sigma_\gamma}{\gamma}$ at the end of modulator. Similarly for the other boxes, except for the sixth one. Since the sixth box stands for the amplifier, there is no dispersion strength $\frac{d\psi}{d\gamma}$, and the relative local energy spread $\frac{\sigma_\gamma}{\gamma}$ is the average value along the amplifier. The effect of the global energy spread (or correlated energy spread, in the terminology of certain other workers in this field) is addressed in the following discussion of the sensitivity to the parameter variation, for its effect is essentially an issue of detuning.

Now, let us explore the physics process in such a device. As shown in Fig. 3, the $2,250$-Å laser, with a peak power of 1 GW, together with the 2-GeV e-beam, is introduced into the modulator of the first stage, where an energy modulation is formed in the e-beam. Then by passing through the following dispersion section, the energy modulation is converted into a spatial modulation. Such a spatially-modulated e-beam is then introduced into the following radiator. Since the radiator is resonant to the fifth harmonic of the seed laser, we will have 450-Å radiation, which is produced by coherent emission followed by an exponential growth into saturation. In order to go to next stage, we need a shifter, in which the e-beam is magnetically delayed. Thus, effectively, the 450-Å radiation is shifted to the front part of the same e-beam, where the e-beam is still "fresh". Because, for the 2 GeV e-beam and the parameters we choose for the undulators, the quantum diffusion effect [38] is negligible, we use a "shifter" to meet the "fresh-bunch" requirement to achieve the best efficiency. Now, the 450-Å radiation serves as the seed laser in the second stage, where the 450-Å radiation input generates a 90-Å output with a power of 1.7 GW. Up to this stage, we are using the lower energy e-beam, and the wavelength is relatively long. In order to achieve high-power x-rays, the 2-GeV e-beam is dumped after this stage, and a 14-GeV e-beam is introduced for the next stage. Now, the 90-Å radiation is the seed laser for the next stage to be converted to 18-Å. Here we would like to emphasize that, for this and for the following fourth and fifth stages, the radiator works in the coherent emission region, i.e. after the coherent emission is finished, the radiation is introduced to the next stage without exponential growth. This makes the total length of the device short. For the 14-GeV e-beam and the parameters we choose for the undulators of each stage, the quantum diffusion effect [38] will lead to a local energy spread growth comparable to the initial local energy spread. Local energy spread growth will degrade the harmonic generation efficiency, we therefore use one bunch for each stage to meet the "fresh bunch" re-

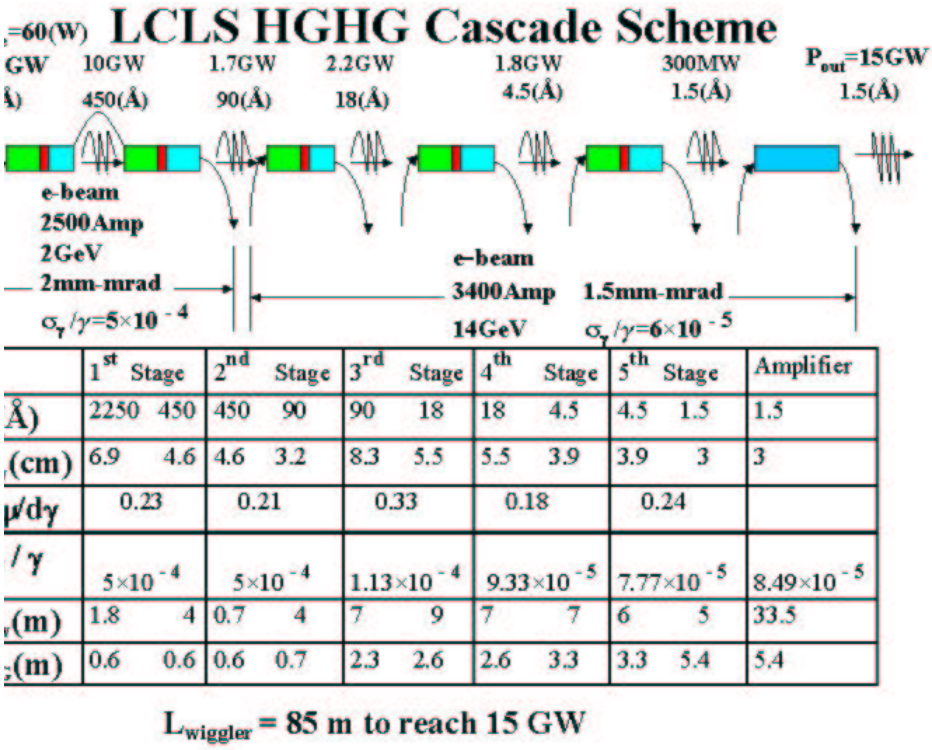

	1st Stage		2nd Stage		3rd Stage		4th Stage		5th Stage		Amplifier
Å)	2250	450	450	90	90	18	18	4.5	4.5	1.5	1.5
(cm)	6.9	4.6	4.6	3.2	8.3	5.5	5.5	3.9	3.9	3	3
μ/dγ	0.23		0.21		0.33		0.18		0.24		
/ γ	5×10^{-4}		5×10^{-4}		1.13×10^{-4}		9.33×10^{-5}		7.77×10^{-5}		8.49×10^{-5}
(m)	1.8	4	0.7	4	7	9	7	7	6	5	33.5
(m)	0.6	0.6	0.6	0.7	2.3	2.6	2.6	3.3	3.3	5.4	5.4

FIG. 3: Schematic plot of the device for producing x-rays with an HGHG-based approach.

quirement to achieve the best efficiency in an ideal study. Hence, after the 18-Å radiation is produced, the e-beam is dumped and a "fresh" bunch is introduced into the next modulator, where the 18-Å radiation interacts with this "fresh bunch" to produce energy modulation. This process is repeated at the 4th and 5th stage. After each stage, the used e-beam is dumped with a new beam introduced for the next stage to reduce the energy spread growth. In the radiator of the 5th stage, right after the coherent emission is finished, the e-beam is also dumped and a "fresh bunch" is introduced to interact with this 1.5-Å radiation in the last undulator, i.e. the amplifier, of the device. In the amplifier, the 1.5-Å radiation interacts with a "fresh" 14-GeV e-beam, and the radiation is amplified exponentially until saturation. Finally, with a total undulator length of about 88 m for the whole device, we will obtain about 15-GW radiation at 1.5-Å, in deep saturation region. We emphasize that, in the radiator of the third, fourth and fifth stage, there is no exponential growth of the harmonic, but rather, after the coherent emission is finished, the harmonic is introduced to the next stage directly. For example, the length of the fifth radiator is only 5 m, while the corresponding power e-folding length without energy modulation is about 5.4 m, so no exponential growth is expected.

We remark here that if we choose the relative local energy spread as the relative global energy spread as 2×10^{-4}, then we can ignore the quantum diffusion effect [38] entirely, and we could just one electron bunch for the 3rd and the 6th stages. calculation leads to a similar system with the total wiggler length increased to about 120 meters, i.e. the increase is not a dramatic one.

When the radiation traverses the shifter, and the connection region where the 2 GeV e-beam is dumped and 14 GeV e-beam is introduced, there is diffraction loss in the radiation. Such diffraction effects are also taken into account for the connection regions of the following stages, where a "fresh" 14 GeV e-beam is introduced and the previous 14 GeV e-beam is dumped. These considerations will be detailed in the following section.

B. Analytic estimate

1. *General criteria*

Now let us give some analytical description of the physics in each stage. As we can see from Fig. 3 (by comparing wiggler length with the power e-folding length), the modulators of all the stages and the radiators in stages 3, 4 and 5 are not working in exponential region. For these sections, we are justified in analyzing the process within small-gain theory. We will give further details of derivation in the following section and in the Appendices, here we give a brief qualitative description.

As what we described in the HGHG principle section, in each HGHG stage, when the electron bunch enters the

radiator, the harmonic contents at the seed laser wavelength and also its high harmonics are abundant. The radiator is designed to be resonant to a special harmonics, therefore coherent emission at this special harmonic is obtained. Suppose we want to get the nth harmonics of the seed laser, then the quantity we need look at is the nth harmonic coefficient of the spatial modulation. The harmonic coefficient is twice of the more frequently used bunch factor. The corresponding bunching factor is [16]

$$\begin{aligned} b_n(r,z) &\equiv \; | < e^{-i\,n\,\theta_j} > | \\ &= \exp\left[-\frac{1}{2}\,n^2\,\sigma_\gamma^2\left(\frac{d\theta}{d\gamma}\right)^2\right]\left|J_n\left[n\,\Delta\gamma\left(\frac{d\theta}{d\gamma}\right)\right]\right| \\ &= \exp\left[-\frac{1}{2}\,\sigma_\gamma^2\left(\frac{d\psi}{d\gamma}\right)^2\right]\left|J_n\left[\Delta\gamma\left(\frac{d\psi}{d\gamma}\right)\right]\right| \quad (1) \end{aligned}$$

where $\theta = (k_r + k_w)z - \omega_r t$ is the ponderomotive phase of the e-beam in the modulator; k_r and ω_r are the seed laser wave number and frequency, respectively; $k_w = \frac{2\pi}{\lambda_w}$, and λ_w is the period of the modulator; $\psi = n\,\theta$ is the ponderomotive phase in the radiator; $\Delta\gamma$ is the energy modulation produced in the modulator, and σ_γ is the rms local energy spread.

Since, in the bunching factor, the exponential part is monotonous, if we want to optimize the system, we try to adjust the parameter so that $J_n[x]$ is near its maximum. Empirically, knowing that $J_n[x]$ peaks around $x \sim 1.2\,n$, gives us the first criterion in the design,

$$\Delta\gamma\left(\frac{d\psi}{d\gamma}\right) \approx 1.2n \quad (2)$$

Now, the exponential part in the bunching factor reads,

$$\exp\left[-\frac{1}{2}\sigma_\gamma^2\left(\frac{1.2n}{\Delta\gamma}\right)^2\right]. \quad (3)$$

Obviously, we need the energy modulation to dominate the energy spread to get a large bunching factor. Thus the first thought might be: the larger the modulation, the better the result. On the other hand, the larger the modulation, the larger the effective energy spread in the electron beam, and this may reduce the radiation power. The exponent of Eq. (3) should be on the order of one, and thus the second criterion is

$$\Delta\gamma \geq n\sigma_\gamma. \quad (4)$$

Equations (2) and (4) are essentially the starting points of all our considerations, though some details need be considered in the real simulation. In the one-stage case as of the experiment [19, 20], Eq. (4) may not be satisfied, because we need to consider also the limit of $\frac{\Delta\gamma}{\gamma} < \rho$, the Pierce parameter [2], to ensure the exponential growth in the radiator. In the Harmonic Generation stages, i.e., in the converter of the cascading scheme [39, 40], exponential growth is not needed. Therefore, $\Delta\gamma$ could be bigger than $n\,\sigma_\gamma$. We will explore this further in the following sections.

2. Modulator

In the modulator, we model the seed laser as a Gaussian TEM_{00} mode [47] centered at Z_W. The interaction between the electron transverse wiggling and the transverse electric field of the seed laser leads to an energy modulation $\Delta\gamma(r,\theta) = \Delta\gamma(r)\sin\theta$, with

$$\Delta\gamma(r) \approx \frac{w_0}{\bar{w}}\frac{a_w[JJ]L_{mod}}{\gamma_0}\mathrm{e}^{-\frac{r^2}{\bar{w}^2}}\frac{1}{mc^2/e}\sqrt{\frac{2Z_0P_{in}}{\lambda_r Z_R}}, \quad (5)$$

where $Z_0 = 120\,\pi\,\Omega$ is the vacuum impedance; P_{in} is the input seed power; λ_r is the seed laser wavelength; γ_0 is the electron's Lorentz factor; L_{mod} is the length of the modulator; $Z_R = \frac{\pi w_0^2}{\lambda_r}$ is the Rayleigh range; and w_0 is the waist diameter of the seed laser. In Eq. (5), $\bar{w}$ is defined as

$$\bar{w}^2 \equiv \frac{1}{L_{mod}}\int_0^{L_{mod}} w^2(z)\,dz, \quad (6)$$

where,

$$w^2(z) = w_0^2\left[1 + \frac{(z - Z_w)^2}{Z_R^2}\right]. \quad (7)$$

We must also take the optical guiding mechanism [48, 49] into consideration. Since the seed laser has extremely high peak power, optical guiding is achieved within a very short interaction time. Once optical guiding is achieved in the linear region, the FEL beam size stays almost constant. Hence, in Eq. (5), we need replace $\bar{w}$ with $w(0)$, i.e., the laser beam size at the entrance of the modulator.

For a planar undulator, the Bessel factor $[JJ]$ is given by

$$[JJ] = J_0\left[\frac{a_w^2}{2(1+a_w^2)}\right] - J_1\left[\frac{a_w^2}{2(1+a_w^2)}\right], \quad (8)$$

where $a_w \equiv \frac{K}{\sqrt{2}}$ is the rms dimensionless undulator vector potential.

Now, let us design the modulator. Given an e-beam, σ_γ is given. Therefore, according to Eq. (4), we know how large an energy modulation we need in order to induce enough spatial modulation after the dispersion section. Then according to Eq. (5), we get the length of the modulator as a function of given input seed power. Once the input power is given, the length of the modulator could be estimated. Since the eigenmode of the FEL is neither a plane wave nor a focused Gaussian beam, Eq. (5) can provide only an estimate for the length of the modulator, though this estimate agrees with numerical simulation fairly well.

3. Dispersion Section

3.1 Dispersion Strength

In order to convert the energy modulation obtained in the modulator into a spatial modulation we need a dispersion section. The phase advance introduced in the dispersion section is then

$$\Delta\psi_{disp}(r) \approx \frac{d\psi}{d\gamma}_{disp} \Delta\gamma(r) \tag{9}$$

A few comments have to be added here, when we use this criterion in the numerical simulation, we need also consider the effective dispersion in the modulator, and in the lethargy region of the radiator. According to the pendulum equations, the effective phase advance introduced in the modulator would be

$$\Delta\psi_{mod}(r) \approx n\frac{2k_{u\,m}}{\gamma_0}\frac{1}{2}\Delta\gamma(r)L_{mod}\ , \tag{10}$$

where n is the harmonic number; $k_{u\,m} = \frac{2\pi}{\lambda_{u\,m}}$, with $\lambda_{u\,m}$ to be the modulator period. Considering the building up process of the energy modulation $\Delta\gamma$ in the modulator, we put $\frac{1}{2}$ in front of $\Delta\gamma$.

The coherent emission takes place in the lethargy region which is roughly $2L_{G\,r}$ as we will discuss in the following. Here $L_{G\,r}$ is the power e-folding length in the radiator. In this lethargy region where $z < 2L_{G\,r}$, the effective phase advance is,

$$\Delta\psi_{rad}(r,z) \approx \frac{2k_{u\,r}}{\gamma_0}\Delta\gamma(r)\,z\ , \tag{11}$$

where $k_{u\,r} = \frac{2\pi}{\lambda_{u\,r}}$, with $\lambda_{u\,r}$ to be the radiator period. If the radiator is long enough to have exponential growth, then we need set $z = 2\,L_{G\,r}$ in the above equation to compute the total phase advance in the lethargy region of the radiator.

As we will show in the next section, the coherent emission power is proportional to the square of the bunching factor, i.e., $P^{Coh}(z) \propto b_n(r,z)^2$, hence, we hope that the maximum value of the bunching factor is reached at roughly the middle of the lethargy region, i.e. around $z = L_{G\,r}$. Therefore, according to the consideration leading to Eq. (2), we would optimize the dispersion strength in the dispersion section according to

$$\Delta\psi_{mod}\left(r=\frac{\sigma_\perp}{\sqrt{2}}\right) + \Delta\psi_{disp}\left(r=\frac{\sigma_\perp}{\sqrt{2}}\right) + \Delta\psi_{rad}\left(r=\frac{\sigma_\perp}{\sqrt{2}}, z=L_{G\,r}\right) \approx 1.2\,n\ , \tag{12}$$

i.e.,

$$\frac{d\psi}{d\gamma}_{disp} \approx -\frac{nk_{u\,m}L_{mod}}{\gamma} + \frac{1.2\,n}{\Delta\gamma\left(r=\frac{\sigma_\perp}{\sqrt{2}}\right)} - \frac{2k_{u\,r}L_{G\,r}}{\gamma}\ , \tag{13}$$

where $\sigma_\perp = \sigma_x = \sigma_y = \frac{\sigma_r}{\sqrt{2}}$ is the transverse rms size of the electron beam. We choose the energy modulation to be the value at $r = \frac{\sigma_\perp}{\sqrt{2}}$ because the energy modulation is not constant across the e-beam.

All these analytical considerations are the guidance in our design. The dispersion strength given in Eq. (13) serves as an initial try if Eq. (4) is satisfied. Otherwise, if the energy modulation does not dominate the local energy spread, Eq. (13) will not give a good starting estimate. Therefore we must look at the bunching factor as a whole, i.e., we must exam Eq. (1), or in the notation of Eq. (A42) in Appendix A, we need to optimize the bunching fact as a function of $\frac{d\psi}{d\gamma}_{disp}$:

$$\bar{b}_m\left(\frac{d\psi}{d\gamma}_{disp}\right) = \exp\left[-\frac{1}{2}\left(\frac{\sigma_\gamma}{\Delta\gamma\left(r=\frac{\sigma_\perp}{\sqrt{2}}\right)}\right)^2\left[\Delta\psi_{mod}\left(r=\frac{\sigma_\perp}{\sqrt{2}}\right) + \frac{d\psi}{d\gamma}_{disp}\Delta\gamma\left(r=\frac{\sigma_\perp}{\sqrt{2}}\right) + \Delta\psi_{rad}\left(r=\frac{\sigma_\perp}{\sqrt{2}}, z=L_{G\,r}\right)\right]^2\right] \times \left|J_m\left[\Delta\psi_{mod}\left(r=\frac{\sigma_\perp}{\sqrt{2}}\right) + \frac{d\psi}{d\gamma}_{disp}\Delta\gamma\left(r=\frac{\sigma_\perp}{\sqrt{2}}\right) + \Delta\psi_{rad}\left(r=\frac{\sigma_\perp}{\sqrt{2}}, z=L_{G\,r}\right)\right]\right|. \tag{14}$$

This optimization gives a value of $\frac{d\psi}{d\gamma}_{disp}$, which agrees quite well with the simulation result for $\frac{d\psi}{d\gamma}_{disp}$. As we will discuss in the following section, we also have to consider the stability of the system, and we need further "over-tune" the dispersion strength.

3.2 Emittance Effects

In the dispersion section, the emittance-induced phase mixing is far smaller than that due to the local energy spread [31]. This is the key point why in the HGHG scheme, the emittance will be a less important factor, and it suggests a new operation mode, i.e., higher current, though unavoidably with higher emittance. To illustrate this, let us compute an ideal case, i.e., we assume that the idealized dispersion section is divided into three sections

with a total length L_d, the field is

$$B(z) = \begin{cases} B & 0 \le z < \frac{L_d}{4} \\ -B & \frac{L_d}{4} < z < \frac{3L_d}{4} \\ B & \frac{3L_d}{4} < z \le L_d \,. \end{cases} \tag{15}$$

In such dispersion section, both the emittance ϵ and the local energy spread σ_γ of the electron bunch lead to a path length difference. The emittance acts like an effective relative local energy spread of [43]

$$\left.\frac{\sigma_\gamma}{\gamma}\right|_{eff,\epsilon}^{disp} = \frac{48R^2\epsilon}{L_d^2\beta}, \tag{16}$$

where R is the bending radius; $\beta = \frac{\lambda_\beta}{2\pi}$, with λ_β to be the betatron motion period.

In the undulator, there is also a natural dispersion as in Eqs. (10) and (11). The emittance acts like an effective relative local energy spread, which is [43]

$$\left.\frac{\sigma_\gamma}{\gamma}\right|_{eff,\epsilon}^{undul} = \frac{\lambda_w\epsilon}{2\lambda_s\beta}. \tag{17}$$

Let us analyze the device in Fig. 3. Shown in Table I are the effective relative local energy spread due to the emittance in the dispersion sections and the undulators in each stage. In our calculation, we use $L_d = 0.32$ m. There are 5 stages as in Fig. 3; "Mod." stands for the modulator, "Disp.," the dispersion section and "Rad.," the radiator. We found that the effective relative local energy spread due to the emittance in the dispersion section is far smaller than that in the undulators. Hence, by reducing the undulator length, the emittance effect is greatly reduced. This is called the Natural Emittance Effect Reduction (NEER) mechanism. The NEER mechanism suggests a new operation mode, i.e., we could use an electron bunch with a higher current, even though unavoidably higher emittance, in the Harmonic Generation stages, i.e., in the converter, though in the amplifier we would still use a low-emittance electron beam. Detailed investigation is underway [43].

4. Radiator

4.1 Start-up Coherent Emission Power

For the radiator, the energy modulation from the modulator makes the effective energy spread in the electron beam larger, so that the power e-folding length L_G increases accordingly. Hence as long as the radiation power from the coherent radiation is large enough for the next stage, there is no need for exponential growth. The length of the radiator is chosen to just reach the power required for the modulation of the next stage.

In the HGHG scheme, the electron beam is spatially bunched after passing through the dispersion section. A bunched beam has abundant spatial harmonics, so the radiations at the fundamental frequency and its harmonics are greatly enhanced. In the Appendix A, we give some brief derivation for such radiation.

If the radiator is resonant to the mth harmonic of the seed laser in the modulator, then, according to the derivation in Appendix A, we know

$$P_1^{Coh}(z) = \frac{Z_0\, I_{peak}^2}{8}\frac{1}{4\pi\sigma_x^2}\left(\frac{K\,[JJ]}{\gamma}\right)^2\left(\int_0^z \bar{b_m}(z)\,dz\right)^2, \tag{18}$$

where $I_{peak} = N_e\, e_0/L_t$, and $\bar{b_m}(z)$ is the average of the bunching factor over the transverse area, and it is given by Eq. (A42) in Appendix A.

As we show in Appendix B, the start-up region is about the first two power e-folding length. If the radiator is shorter than $2\,L_{G\,r}$, we would use Eq. (18) to compute the coherent emission power, but if it is longer than $2\,L_{G\,r}$, we need to use the Eq. (19), below, for the exponential growth region.

4.2 Amplified Guided Mode

The coherent emission has finite bandwidth as we discussed in Appendix A, hence the question of how much coherent emission power is coupled into the guided mode [6, 48, 49] needs to be addressed. In Appendix B, we give some brief derivation on this question. The guided mode has a peak power of

$$P_{00}^{Guided} = C_{00}P_1^{Coh}(z = 2\,L_{G\,r})\,e^{\frac{z}{L_{G\,r}}}, \tag{19}$$

where C_{00} is the coupling coefficient. The physics meaning of Eq. (19) is clear. The coherent emission in the first two power-e-folding length serves as the start-up power. This amount of coherent emission power is coupled into the guided mode with a coefficient of C_{00}. Then this amount of power is amplified further in the undulator. In Appendix B, we give some derivations. An estimate for a large e-beam limit gives $C_{00} \approx \frac{3.71}{12} \approx \frac{1}{3}$. A more careful estimate puts $C_{00} \approx \frac{1}{5}$. The similar question of how much incoherent noise power is coupled into the guided mode has been studied [6, 10, 50] for the SASE FEL.

4.3 Exponential Growth Region

As shown in Eq. (19), after the coherent emission is finished, the system goes into the exponential region. Again, it is seen that the lethargy region is around $2\,L_{G\,r}$ for $C_{00} \approx \frac{1}{5}$ as in the Appendix B.

Since there is energy modulation after the modulator, the local energy spread no longer has its initial value. Here we use an effective energy spread to take this energy modulation into account,

$$\left.\frac{\sigma_\gamma}{\gamma}\right|_{eff} = \sqrt{\left(\frac{\sigma_\gamma}{\gamma}\right)^2 + \left(\frac{\Delta\gamma(r = \frac{\sigma_\perp}{\sqrt{2}})}{\sqrt{2}\,\gamma}\right)^2}, \tag{20}$$

Stage 1			Stage 2		
Mod.	Disp.	Rad.	Mod.	Disp.	Rad.
3.1×10^{-5}	1.0×10^{-5}	1.0×10^{-4}	1.0×10^{-4}	5.5×10^{-5}	3.6×10^{-4}
Stage 3			Stage 4		
1.4×10^{-5}	3.6×10^{-7}	4.5×10^{-5}	4.5×10^{-5}	2.6×10^{-6}	1.3×10^{-4}
Stage 5					
1.3×10^{-4}	5.9×10^{-6}	3.0×10^{-4}			

TABLE I: The effective relative local energy spread σ_γ/γ due to the emittance ϵ of the electron beam.

where $\Delta\gamma(r)$ is given in Eq. (5). Then $L_{G\,r}$ is the power e-folding length in the radiator or the final amplifier based on this effective relative local energy spread. $L_{G\,r}$ could be found analytically from the scaling function [7, 51] for a water-bag model. Or, for a Gaussian Model, one could get the value, based on a 19-parameter polynomial fitting formula [52].

4.4 Saturation Power and Radiator Length

In order to estimate the radiator or the amplifier length, we need know the saturation power. The saturation power obtained empirically by fitting simulation results is given by [53],

$$P_{sat} \approx 1.6\rho \left(\frac{L_{G\,r,1D}}{L_{G\,r}}\right)^2 P_{b,pk}. \tag{21}$$

Here $P_{b,pk} = I_{peak}\gamma\frac{m\,c^2}{e}$ is the total peak beam power, and $L_{G\,r,1D} = \frac{\lambda_{u\,r}}{4\pi\sqrt{3}\rho}$ is the 1-D power e-folding length.

Therefore, if we design the system so that the radiator extends to the saturation region, then the length of the radiator could be estimated by solving

$$P_{00}^{Guided}\left(z = L_{rad}\right) = P_{sat}, \tag{22}$$

i.e.,

$$L_{rad} \approx L_{G\,r} \ln\left[\frac{8\rho P_{pk}}{P_1^{Coh}\left(z = 2\,L_{G\,r}\right)}\left(\frac{L_{G\,r,1D}}{L_{G\,r}}\right)^2\right], \tag{23}$$

for $C_{00} \approx \frac{1}{5}$ in Eq. (19).

With such a straightforward analytical estimate, we could check the numerical simulation results from upgraded version [46] of TDA [55]. The analytical estimate, though very rough, agrees with the TDA numerical simulation within a factor of 2, which seems reasonable.

5. Shifter, Connection Region and Rayleigh Range of the FEL

So far, we have described the details for designing one complete stage, i.e. a modulator, the dispersion section, and then the radiator. In the cascading scheme [39–41], we use a "fresh-bunch technique" [44] either to shift the light to a fresh part of the e-beam or to dump the e-beam of the current stage and introduce a new e-beam for the following stage. In these connection spaces, we need to consider the diffraction effect.

If we want to shift the light pulse for a distance of ΔS with respect to the electron bunch, the corresponding length of the shifter, L_s reads,

$$L_s = \left[\frac{96\Delta S\gamma_0^2 m^2 c^2}{e^2 B^2}\right]^{\frac{1}{3}}. \tag{24}$$

As usual, we assume an idealized dispersion section as given by Eq. (15).

For the connection part, suppose we need bend the e-beam Δx vertically, then the corresponding longitudinal drift distance S is

$$S = \sqrt{\frac{2\Delta x\gamma_0 mc}{eB_b}}, \tag{25}$$

where we apply a field B_b for bending the e-beam.

According to Eq. (7) of Ref. [7], the fundamental mode of the FEL is assumed to be a Gaussian within the e-beam, and a Hankel function outside the e-beam. Hence, once we found the fundamental mode, we know the Rayleigh range and the waist position of the FEL. These numbers are used in our simulation.

As we are now equipped with analytical estimate for all the details, we could use numerical simulation to get the design done.

IV. STABILITY AND SENSITIVITY TO PARAMETER VARIATION

A. Design thought

We need check the stability of the performance of this system. For each stage, the fluctuation in any parameter of the e-beam, or the seed laser, will lead to the fluctuation of the output power of the harmonic at the end of the radiator. But this output harmonic is the input seed laser for the next stage. Therefore, the fluctuation in the output power of the harmonic in one stage is just the fluctuation in the input power of the seed laser for the next stage. Thus the stability consideration could be

simplified, i.e. we need only check whether each stage of the HGHG could reduce the fluctuation. To be more explicit, we need to check whether the fluctuation of the output power of the harmonic in each stage is less than the fluctuation in the input power of the seed laser of the same stage.

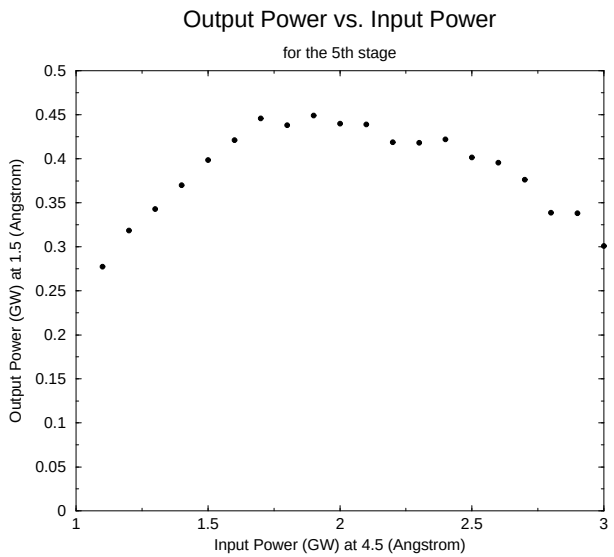

FIG. 4: The relation between the output power change and the input power change in the fifth stage. The fluctuation in the output power is only about 20% when the input power changes from 1 GW to 3 GW. This is an attractive feature of the HGHG scheme.

In Fig. 4, we plot the relation between the output power and the input power for the fifth stage. The fluctuation in the output power is only about 20%, when the input power changes from 1 GW to 3 GW. This is an attractive feature of the HGHG scheme. For the first, second, third and fourth stages, the variation of a factor 3 in input power (like that in the fifth stage) generates an output fluctuation of 10%, 15%, 45% and 30% respectively. This result is a trade-off between better stability and total wiggler length, i.e., if we use a lower harmonic number and add one more stage, the stability will be further improved. Analytical study described in the following section shows that such attractive feature holds as long as the harmonic number is not too high. Therefore, in our scheme, we use harmonic number, 3, 4 and 5. As each stage reduces the fluctuation, we could expect that the radiation fluctuation caused by the fluctuation in the parameters of the preceding stage will be stabilized in the following stage. Therefore, not much fluctuation is expected after all five stages. Thus the stability of the whole system is determined mostly by the last amplifier. Fig. 5 shows its performance in the amplifier. Since the amplifier is only 33.5 m long, which should be compared with the 100 m long undulator in the SASE scheme [54], the stability of the HGHG scheme is expected to be better than that of the SASE scheme. The results of the calculation confirmed this.

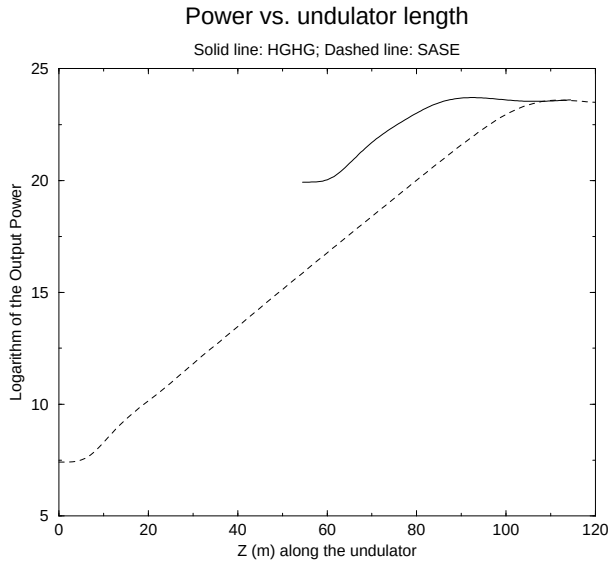

FIG. 5: The radiation power along the device. The solid line indicates the radiation power in the last amplifier of the HGHG scheme. The radiation power of the previous stages is not plotted. The dashed line shows data for the SASE scheme. The performance at 85 m for the HGHG scheme is similar to that at 110 m for the SASE scheme.

B. Analytic consideration

In order for the system to have good performance, we need to consider the stability. Let us reexamine the bunching factor, i.e. Eq. (1). The exponential part is monotonous but since the Bessel function has a peak, we can make use of this property. In the bunching factor, for a given e-beam, σ_γ is fixed, and we are left with two free parameters to adjust: $\Delta\gamma$ is a property from the modulator, and $\frac{d\psi}{d\gamma}$ is related to the dispersion section. For simplicity, we set $x = \Delta\gamma(\frac{d\psi}{d\gamma})$, and we set $n = 5$; the $J_5[x]$ curve is plotted in Fig. 6. Our first thought would be to adjust x, so that $J_5[x]$ reaches maximum, i.e. we would like put $x \approx 6.4$. Now, recall that

$$\Delta\gamma \propto \sqrt{P_{in}}, \tag{26}$$

according to Eq. (4). While according to Eqs. (18) or (19) and (1), we know

$$P_{out} \propto b_n^2 \propto (J_n[x])^2 . \tag{27}$$

Now, suppose that $\frac{d\psi}{d\gamma}$ is tuned so that for an input power P_{in}^{peak},

$$\Delta\gamma^{peak}(\frac{d\psi}{d\gamma}) = 6.4, \tag{28}$$

where $\Delta\gamma^{peak}$ is the energy modulator produced by P_{in}^{peak}. Based on the same $\frac{d\psi}{d\gamma}$, we could compute the output power, if the input power is $P_{in}^{e^{-1}} = e^{-1}P_{in}^{peak} \approx \frac{1}{3}P_{in}^{peak}$. Now, let us compute the ratio of the two radiation power. We have

$$R_n \equiv \frac{P_{out}^{e^{-1}}}{P_{out}^{peak}} = \frac{(J_n[\sqrt{e^{-1}}\Delta\gamma^{peak}(\frac{d\psi}{d\gamma})])^2}{(J_n[\Delta\gamma^{peak}(\frac{d\psi}{d\gamma})])^2}. \tag{29}$$

When the dispersion is tuned so that Eq. (28) is satisfied for $n = 5$, we have $R_5 \approx 8\%$. The system is very delicate, since we need to use multiple stages, and the fluctuation in each stage will affect the next stage and so on. If we optimize the system according to Eq. (28), we would require very small fluctuation in the system. A direct way to overcome this problem is to make the radiator longer, so that the exponential growth region will be reached. Now, if the input power is smaller, so is the energy modulation. The coherent radiation is smaller, but the effective energy spread due to the energy modulation is smaller, so the power e-folding length is shorter. This means that the radiation will grow faster, so somewhere in the radiator, the smaller input power curve will cross the bigger input power curve as in Fig. 7. Thus, if the power e-folding length of the FEL is small, we would like to make the radiator longer, and even let it go to the saturation region, where the fluctuation is expected to be small. This is how we would stabilize the first stage. But, if we want to go to x-ray, the power e-folding length gets large, $L_{G\,r} = 5.4\,m$, for 1.5-Å radiation without energy modulation. Because of the effective energy spread due to the energy modulation, $L_{G\,r}$ could be even longer. Therefore, making the radiator longer to ensure stability is not that practical in reaching x-ray. But, according to Fig. 6, if we overtune the dispersion so that $\Delta\gamma^{peak}(\frac{d\psi}{d\gamma})$ is larger than 6.4, $J_5[\Delta\gamma^{peak}(\frac{d\psi}{d\gamma})]$ will drop while $J_5[\sqrt{e^{-1}}\Delta\gamma^{peak}(\frac{d\psi}{d\gamma})]$ will become large, so we can make these two numbers equal, i.e. we could get $R_n = 1$. Or equivalently, we need to solve

$$J_n[x^{peak}] = J_n[\sqrt{e^{-1}}x^{peak}], \tag{30}$$

where $x^{peak} = \Delta\gamma^{peak}(\frac{d\psi}{d\gamma})$, to find the right $\frac{d\psi}{d\gamma}$ for a given $\Delta\gamma^{peak}$. Equation (30) tells us that a factor of 3 difference in the two input power will produce the same coherent radiation output power. Now, let us look at the fluctuation in the output power for this $\frac{d\psi}{d\gamma}$. Since we overtuned the dispersion, the maximum output power will be produced by some input power smaller than that for $\Delta\gamma^{peak}$. Let us introduce

$$\eta_n \equiv \frac{P_{out}^{peak}}{(P_{out})_{max}} = \frac{(J_n[\Delta\gamma^{peak}(\frac{d\psi}{d\gamma})])^2}{(J_n[\Delta\gamma(\frac{d\psi}{d\gamma})])^2_{max}}. \tag{31}$$

In the above formula, ^{peak} stands for the "peak" in the input power, while the $_{max}$ stands for the "maximum" in the output power in the case of overtuned dispersion. We found that $\eta_5 \approx 40\%$, $\eta_4 \approx 50\%$, and $\eta_3 \approx 60\%$. Recall that in such "overtuning" scheme, we would have $R_n = 1$, so the input power varies 3 times from P_{in}^{peak} drops to $P_{in}^{e^{-1}} = e^{-1}P_{in}^{peak} \approx \frac{1}{3}P_{in}^{peak}$. Therefore, the fluctuation in the output power is smaller than that in the input power for $n \leq 5$.

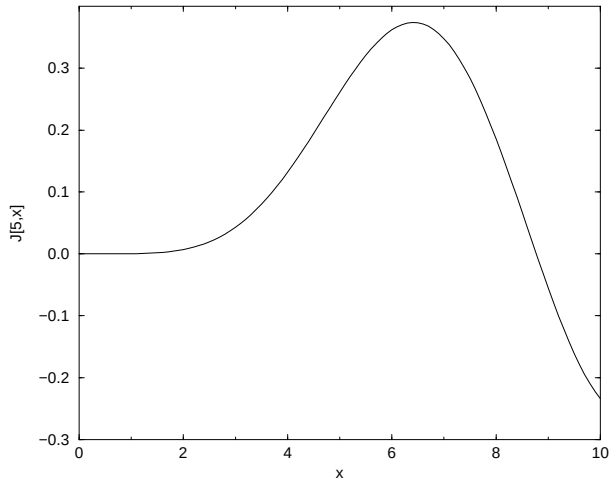

FIG. 6: The fifth-order Bessel Function $J_5[x]$.

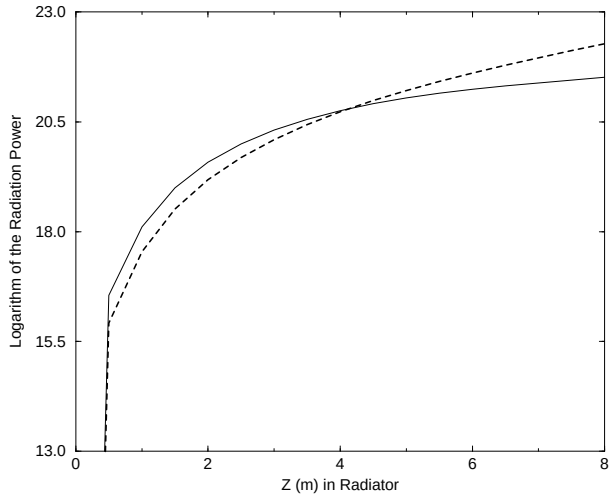

FIG. 7: Demonstration of the situation described in the text. The dashed line stands for smaller input power, and therefore smaller energy modulation, and smaller coherent radiation in the radiator. But, since smaller energy modulation results in smaller effective energy spread, this curve grows faster in the exponential region. The solid curve stands for the opposite situation.

Since the energy modulation also varies across the transverse section of the e-beam, the "over-tuning" mechanism also smoothes the transverse profile of the radiation. For a focused Gaussian seed laser, the on-axis part

of the e-beam has the largest energy modulation, and the outside part of the e-beam has a smaller energy modulation. A right strength of $\frac{d\psi}{d\gamma}$ will lead to overbunching on-axis, best bunching at some part of the e-beam, and under-bunching at the outside part. But the radiation produced by some of the outside part could be the same as that produced by the on-axis part. Therefore the radiation becomes flat, especially after multistage. Shown in Fig. 8 is the output radiation profile for the 4.5-AA to 1.5-AA single stage, where a focused Gaussian seed laser at 4.5-AA produces a flatter radiation pulse at 1.5-AA. This transverse smoothing mechanism leads to a larger Rayleigh region and reduces the diffraction loss in the connection region.

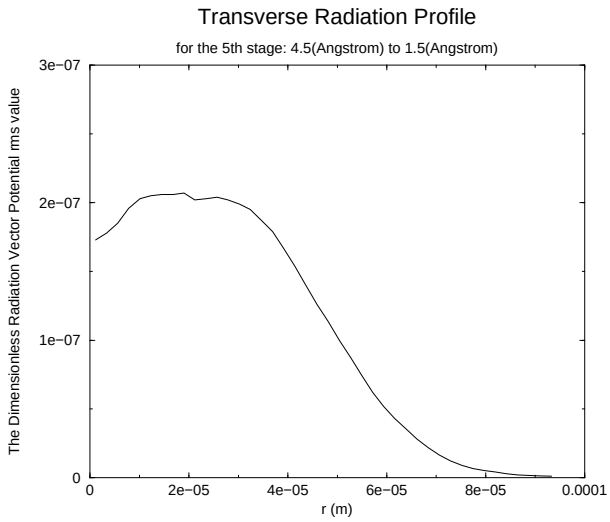

FIG. 8: The transverse profile of the 1.5-AA radiation at the fifth stage, assuming the input 4.5-Å radiation is a focused Gaussian beam, demonstrating the transverse smoothing effect due to the "overtuning" mechanism.

The fluctuation in the global or local energy spread, the current, and the emittance will all result in the fluctuation in the output power, which is the input power of the next stage; therefore, by overtuning the dispersion strength, all such fluctuation could be treated in the same way, and all get stabilized. Thus in such overtuning scheme, the negative input effect, could produce positive output effect.

V. RESULTS

Our calculation was carried out by a modified version [16, 46] of TDA code [55], together with an analytical estimate presented in this paper. For each stage, the analytical estimates agree with the simulation to within a factor of 2. In the calculation, we also consider the diffraction effect of the laser when it traverses the "shifter", and the connection regions between stages. In our calculation, we assume the bending magnet field is $B = 2$ Tesla; therefore, to achieve a deflection such that at the entrance to the next stage the e-beam is displaced by 5 cm, the connection region is about 1.55 m for the 14-GeV e-beam and 0.58 m for the 2-GeV e-beam. Hence the connection region should be designed with length $L_c = 1.55$ m. If we assume that between the 1st and 2nd stage, the 2-GeV electron bunch needs to be delayed for 50 fs, then, for the same magnet field $B = 2$ Tesla, the "shifter" should be of length $L_s = 25$ cm. These are the numbers used in our calculation. As we mentioned before, the local energy spread growth [38] of the e-beam when it traverses the undulators is also taken into account in our calculation. For example, after the modulator of the 4.5-Å to 1.5-Å stage, the relative local energy spread is increased from 6×10^{-5} to 8×10^{-5}. This decreases the efficiency of harmonic generation slightly. The local energy spread growth in the last amplifier for 1.5-Å is larger, but its effect on the exponential growth of the radiation is negligible. Now let us present the results and some discussion.

To test the stability, we check the sensitivity of the output to the peak current, the initial relative local energy spread, the relative global energy detune, and the normalized emittance. For example, for the first stage, we varied each of these four parameters of the e-beam independently to obtain a range of the output power variation of the harmonic (the 450-Å radiation) at the end of the first stage. In so doing, we obtained the fluctuation in the input power of the seed laser (the 450-Å radiation) for the second stage. Such input power fluctuation will lead to a smaller fluctuation in the output power of the harmonic at 90 Å. This is similar to what we have shown in Fig. 4. But, since the parameters of the e-beam in the second stage fluctuates, we varied each of these four parameters independently again to get a whole range of the output power fluctuation of the harmonic (the 90-Å radiation). Thus the total fluctuation we considered in the output power for each stage is produced by the fluctuation in each of the parameters of the e-beam as well as the input power of the seed laser for each stage. The 90-Å radiation is the seed laser for the third stage, and the fluctuation in the input power leads to smaller fluctuation of the output power at the end of the third stage. But again we needed to vary each of the parameters of the e-beam for a whole range of output power fluctuations of the harmonic (the 18-Å radiation). Repeating the same procedure, we finally obtained the fluctuation of the 1.5-Å radiation.

The output power of each stage has a fluctuation range which leads to a range of the energy modulation fluctuation at the end of the modulator of the next stage. The dispersion strength is adjustable. If we want to optimize the system, then we should tune the dispersion strength so that the largest energy modulation will be favored. In this way, the radiator will produce the most coherent emission, and thus works at the best point. However, in order to get good stability, we will overtune the dispersion strength, so that the largest energy modulation will

produce overbunching in the e-beam, but medium energy modulation will produce best spatial bunching. By such "overtuning" for the dispersion strength, in the smallest energy modulation case, the e-beam is underbunched, and radiation rises slowly in the beginning, but continues growing till the end of the radiator, whereas in the largest energy modulation case, the e-beam is overbunched, and radiation grows fast at first, but later drops. As a result, the smallest energy modulation will produce a similar amount of coherent radiation as does the largest energy modulation. Once the dispersion strength is fixed, the fluctuation range of the radiation is a function of the radiator length, for example, as shown in Fig. 9 for the 2nd stage. We then determine the length of the radiator to be where the fluctuation of the output power is minimum, thus the radiator length for this 2nd stage should be around 4 m.

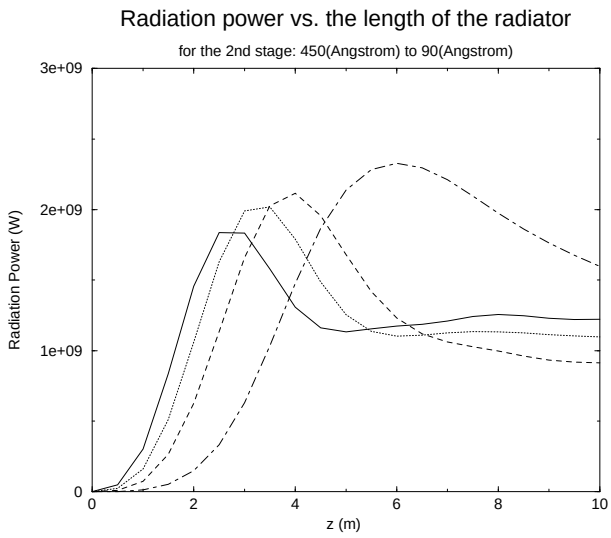

FIG. 9: The radiation power along the 2nd radiator for different values of input power, showing that the output fluctuation is minimum at around 4 m. The solid curve is for input power P_{in}^{solid}; the dotted line: $P_{in}^{dotted} = e^{-0.25} \times P_{in}^{solid}$; the dashed line: $P_{in}^{dashed} = e^{-0.5} \times P_{in}^{solid}$; and the dot-dashed line: $P_{in}^{dot-dashed} = e^{-1} \times P_{in}^{solid}$.

With this choice of radiator length, the large fluctuation in the input power will result in a small fluctuation in the output power as long as the harmonic number is not too high in the harmonic generation, as shown in the Fig. 4.

Thus we trade off the best performance point for a stability in the performance. If the fluctuation in the parameters of the e-beam is small, then we could pursue the best performance point; if so, the total device will be less than 70 m long.

The sensitivity of the output power to the e-beam parameters is plotted in Figs. 10 to 13 for the initial relative local energy spread $\frac{\sigma_\gamma}{\gamma}$, the relative global energy detuning $\frac{\delta\gamma}{\gamma}$, the peak current, and the normalized emittance ϵ_n respectively. If we set the limit of the peak-to-peak output power fluctuation to be within 50% at the end of the whole system, then the tolerance of the parameters will be the following. For the initial local energy spread, $\frac{\sigma\gamma}{\gamma}$ could vary from 6×10^{-5} up to about 9×10^{-5}; for the global energy spread (its effect corresponds to a detuning), $\frac{\delta\gamma}{\gamma} \approx 2\rho$, where $\rho = 4 \times 10^{-4}$, is the Pierce parameter [2] in the 1.5-Å amplifier; for the current, the peak-to-peak fluctuation, $\frac{\Delta I_{pk}}{I_{pk}} \approx 40\%$; for the normalized emittance, ϵ_n could vary from $1.5\,\pi\,mm - mrad$ to about $1.8\,\pi\,mm - mrad$. Tolerance for the 2-GeV part of the system is much more relaxed.

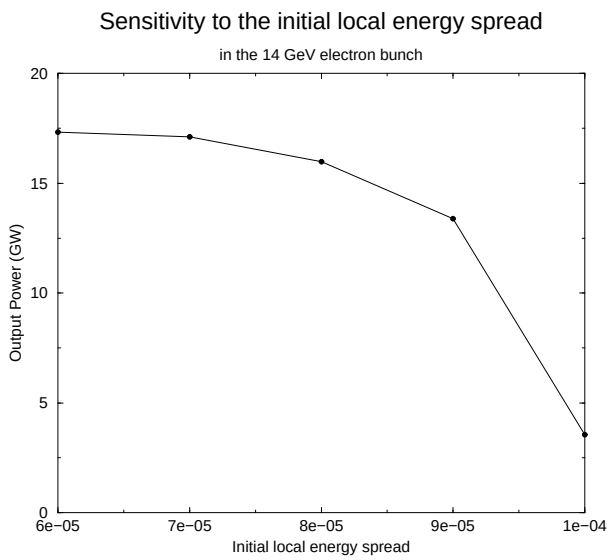

FIG. 10: The sensitivity of the output power to the initial local energy spread.

We now discuss the output as a function of the current as shown in Fig. 12. When the current is less than the nominal value $3,400$ Amp, the behavior is almost monotonic; when the current is larger, but by not too much, there is some oscillation around the mean value. This is because when the current is larger than the nominal value, in one of the five HGHG stages, larger current produces larger output power, which will lead to overbunching in the radiator of the next stage, and less output power will be produced. Thus the input power to the last amplifier could be less than that produced by the nominal value, $3,400$ Amp. Therefore, the final output power could be less, even though the last amplifier will monotonically produce larger output power with larger current. This is what we observed when the current is +5%, +15%, and +20% larger than the nominal value in Fig. 12. Thus the scheme provides the stability of the system based on overtuning.

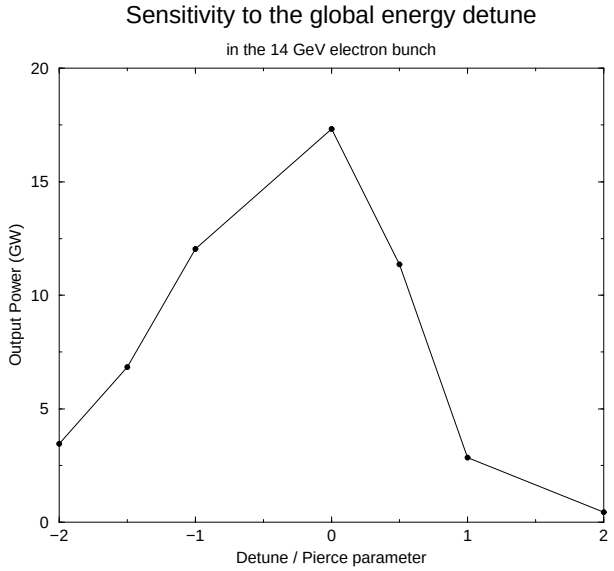

FIG. 11: The sensitivity of the output power to the global energy detune in units of the Pierce parameter ρ[2].

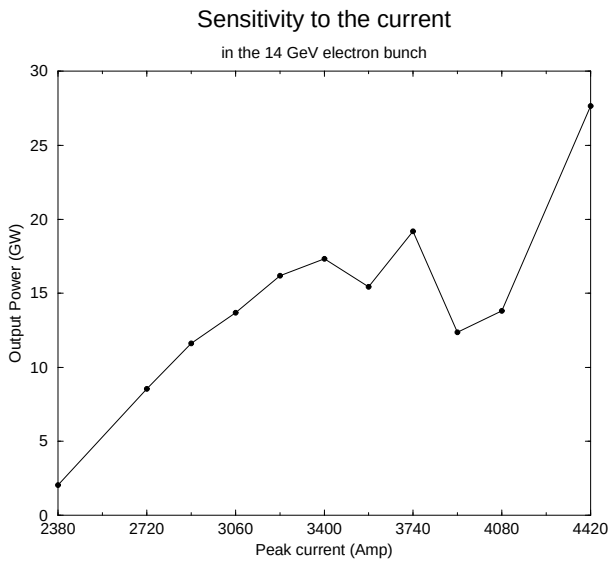

FIG. 12: The sensitivity of the output power to the current fluctuation. $I_{pk} = 3,400$ Amp is the nominal value.

VI. DISCUSSION AND CONCLUSION

A. Total Length

Taking all the fluctuation into consideration, to get an output power of about 15 GW the HGHG scheme will require a total undulator length of 85 m, whereas the corresponding SASE scheme need 100 m according to the design report [54]. If the fluctuation is fairly small, i.e. assuming everything works in the ideal status, the HGHG undulator could be shorten to less than 70 m.

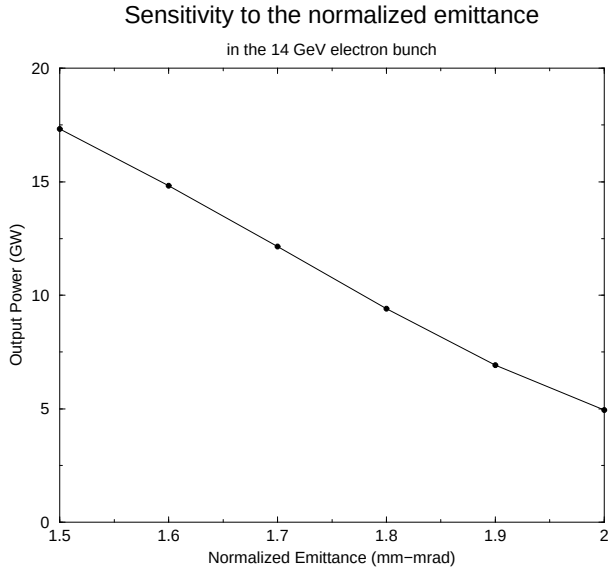

FIG. 13: The sensitivity of the output power to the normalized emittance.

This advantage agrees with previous study [36].

B. Performance

As discussed in Sections IV and V, the performance of the HGHG FEL will be very stable. Fluctuations in any parameters will lead to the fluctuation of the output power of the current stage, which is the fluctuation of the input power to the next stage. As discussed in Section IV, such fluctuation could be reduced based on the "overtuning" scheme. Hence, this intrinsic property of the HGHG scheme guarantees the stability of the performance.

C. Pulse length, pulse shape and spectrum

To calculate the pulse length of the final output, we assume the input seed laser of $2,250$ Å is a Gaussian pulse, with $\sigma_t = 10\,fs$. In Fig. 14, we plot the final output pulse shape. Considering that the radiation pulse overlaps only a small part of the whole electron bunch which is 250 fs long, in our calculation we assume the e-beam parameters remain constant except that there is an energy linear chirp of 1.5% / mm for the 14-GeV e-beam as part of the global energy spread. For comparison, we include a plot of the input Gaussian pulse; both pulse are normalized. Amazingly, we find that such an HGHG device could produce a more or less rectangular pulse of 40 fs long. Again, this is due to our "overtuning" scheme because, in every stage of HGHG, the variation of the output power is reduced. As discussed in Sec. IV B, transversely, the radiation profile is also flattened due

to this "overtuning" mechanism; after multistage, it is more or less like a plane wave, as shown in Fig. 8 for the 4.5-Å to 1.5-Å single-stage example. The spectrum of this pulse has been calculated. The central peak has a relative FWHM bandwidth of about 1.8×10^{-5}. This is to be compared with the LCLS SASE bandwidth of about 7×10^{-4}.

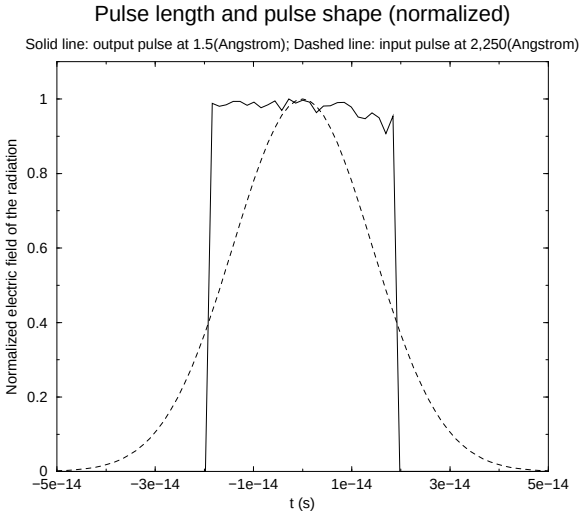

FIG. 14: The pulse shape and pulse length of the final output pulse, with a Gaussian input pulse. Both the output pulse and the input pulse are normalized for comparison.

D. Harmonic Generation without exponential growth

The main part of the HGHG device does not work in the exponential growth region. The modulators are not in that region. For the radiators of the third, the fourth and the fifth stage, they work in the coherent emission region, without exponential growth. As shown in Fig. 3, with a total length of about 50 m, we will achieve several hundred megawatt output power at 1.5 Å. Considering that the bandwidth of the HGHG FEL is much narrower than that of the SASE FEL, even with several hundred megawatt output power, the power spectrum in the HGHG central zone is comparable to that provided by the LCLS SASE scheme.

Because of the NEER mechanism, discussed in Sec. III B. 3.2, we could use a higher-emittance beam. Preliminary result shows that a 14-GeV e-beam with a normalized emittance of $2\,\pi$ mm-mrad does not affect Harmonic Generation much. So relaxing the stringent requirement on the normalized emittance seems possible. By cascading five stages of Harmonic Generation, we will get 1.5-Å radiation with high brightness.

E. High-order Harmonic Generation

Given the high quality of the electron beam proposed in the SLAC LCLS project, our simulation supports a high-order HGHG. For example, we could try 12th harmonics of 18-Å. Then the parameters for that stage would be, 7 m for the modulator, with 18 Å, and then 8 m for the radiator to get about 70 MW output power for 1.5 Å. Then the amplifier needs to be about 38 m to get similar output power, i.e. about 15 GW. Thus the total length will be shortened by about 3.5 m.

F. Harmonics in the last Amplifier

At the end the last Amplifier, the FEL is in the deep saturation region, hence harmonics of this 1.5 Å radiation are also significant. We upgraded [46] the TDA code [55] to implement the calculation for the harmonic contents. The 3rd harmonic, i.e. the 0.5 Å light, will have power up to 30 MW. We believe this will be a good by-product [46, 56]. In Appendix A, analytically, we also discuss the coherent emission power of all the harmonics, even and odd.

G. Conclusion

In conclusion, the cascading HGHG scheme is an attractive scheme for generate coherent x-rays. It will have the advantages mentioned in the beginning of the paper. Among them, the most attractive feature is that the HGHG FEL will achieve much better longitudinal coherence. Such an HGHG scheme seems to be the best candidate for producing short laser pulse, which is an extremely important tool in Chemistry and Biology. Also, the total length will be shorter than the SASE 100 m length. Because of the NEER mechanism, the emittance of the electron beam comes out to be less important, especially in the Harmonic Generation Stages. One other feature is that the device could provide excellent stability.

Acknowledgments

The authors wish to thank Drs. I. Ben-Zvi, S. Krinsky, J.B. Murphy, J.M. Wang of the National Synchrotron Light Source at the Brookhaven National Laboratory; Professor C. Pellegrini of University of California - Los Angeles; Drs. A.W. Chao, P.J. Emma, Z. Huang, H.-D. Nuhn, T.O. Raubenheimer, G.V. Stupakov of Stanford Linear Accelerator Center for many suggestion and comments. Work was supported by US Department of Energy under contract DE-AC03-76SF00515 (JW) and contract DE-AC02-98CH10886 (JW and LHY)

APPENDIX A: COHERENT EMISSION POWER

The energy emitted by an accelerated electron, in MKS unit, is given by [57]

$$\frac{d^2I}{d\omega d\Omega} = \frac{Z_0\, e_0^2\omega^2}{16\pi^3} \times \left|\int_{-\infty}^{+\infty} \hat{\vec{n}} \times \left(\hat{\vec{n}} \times \vec{\beta}(t)\right) e^{+i\omega\left(t-\frac{\hat{\vec{n}}\cdot\vec{r}(t)}{c}\right)} dt\right|^2. \quad \text{(A1)}$$

Here $d^2I/(d\omega d\Omega)$ is the energy emitted per unit frequency and solid angle, $\hat{\vec{n}}$ is a unit vector pointing to the observer of radiation (the detector), $\vec{\beta}(t)$ is the electron's velocity vector and $\vec{r}(t)$ is the electron's position vector. For a group of N_e electrons,

$$\frac{d^2I}{d\omega d\Omega} = \frac{Z_0\, e_0^2\omega^2}{16\pi^3} \times \left|\sum_{j=1}^{N_e}\int_{-\infty}^{+\infty} \hat{\vec{n}} \times \left(\hat{\vec{n}} \times \vec{\beta}_j(t)\right) e^{+i\omega\left(t-\frac{\hat{\vec{n}}\cdot\vec{r}_j(t)}{c}\right)} dt\right|^2 \quad \text{(A2)}$$

Here, we make the small-angle approximation,

$$\hat{\vec{n}} \times (\hat{\vec{n}} \times \beta) = \vec{\beta}_\perp = \hat{\vec{\epsilon}}\beta_\perp, \quad \text{(A3)}$$

with $\hat{\vec{\epsilon}}$ is the polarization of the radiation. We further assume that all the electrons in the beam travel the same trajectory with only their radial positions and starting times being different, we have

$$\vec{r}_j(t) = \vec{r}(t-t_j) + \vec{R}_j, \quad \text{(A4)}$$

where t_j is the starting time for the electron, given by $t_j = -\frac{z_j}{\beta_z\, c} \approx -\frac{z_j}{c}$, $\vec{R}_j$ is perpendicular to $\hat{z}$, and

$$\beta_j(t) = \beta(t-t_j). \quad \text{(A5)}$$

Substituting Eqs. (A3), (A4) and (A5) into Eq. (A2) and making a change of variable $\tau = t - t_j$, we are led to

$$\begin{aligned}\frac{d^2I}{d\omega d\Omega} &= \left|\sum_{j=1}^{N_e} e^{+i\omega t_j} e^{-i\omega\frac{\hat{\vec{n}}\cdot\vec{R}_j}{c}}\right|^2 \frac{d^2I_0}{d\omega d\Omega} \\ &= |F|^2 \frac{d^2I_0}{d\omega d\Omega}. \end{aligned} \quad \text{(A6)}$$

Here $\frac{d^2I_0}{d\omega d\Omega}$ is the radiation produced by a single electron from Eq. (A1), and $|F|^2$ is the coherent enhancement factor [58].

Assuming the electrons are distributed at $t = 0$ according to a number density $n(x, y, z)$, we may rewrite the expression for the coherent enhancement factor as an integral

$$|F|^2 = \left|\int n(x,y,z)\, e^{-ikz}\, e^{-ik\hat{\vec{n}}\cdot\vec{R}} dxdydz\right|^2. \quad \text{(A7)}$$

Now we write $n(x, y, z)$ as an original unbunched electron density times a bunching term,

$$n(x,y,z) = n_0(x,y,z)\left(1 + \sum_{n=1}^{\infty} a_n(x,y)\cos(nk_r z)\right), \quad \text{(A8)}$$

where $k_r = k_u \frac{2\gamma^2}{1+\frac{K^2}{2}+\gamma^2\theta^2}$ is the resonant wavenumber, and $a_n(x, y)$ is the Fourier coefficient for a particular harmonic. Here we assume that the Fourier coefficients are independent of z, i.e., there is no dynamics. We assume initially,

$$\begin{aligned} n_0(x,y,z) &= \frac{N_e}{(2\pi)^{3/2}\sigma_x\sigma_y\sigma_z}\, e^{-\frac{x^2}{2\sigma_x^2}}\, e^{-\frac{y^2}{2\sigma_y^2}}\, e^{-\frac{z^2}{2\sigma_z^2}} \\ &\equiv N_e n_{0x}(x) n_{0y}(y) n_{0z}(z) \end{aligned} \quad \text{(A9)}$$

where σ_x, σ_y and σ_z are the rms beam size, and N_e is the total number of electrons in the bunch. $n_{0x} \equiv \frac{1}{\sqrt{2\pi}\sigma_x} e^{-\frac{x^2}{2\sigma_x^2}}$, and n_{0y} and n_{0z} are similar. If we expand the square in Eq. (A7), drop cross terms, and examine the nth term, we have

$$|F_n|^2 = \left|N_e \int dxdydz\, n_{0x}(x) n_{0y}(y) n_{0z}(z) a_n(x,y) e^{-ik(n_x x + n_y y)} e^{-ikz} \cos(nk_r z)\right|^2. \quad \text{(A10)}$$

After completing the integral for x, y and z, we have

$$|F_n|^2 = \frac{\sigma_{n\perp eff}^4}{\sigma_\perp^4} a_{n0}^2 N_e^2 \left\{ \left| \frac{1}{2} e^{-\frac{\sigma_z^2}{2}(k-nk_r)^2} \, e^{-\frac{1}{2}k^2(n_x^2+n_y^2)\sigma_{n\perp eff}^2} \right|^2 + \left| \frac{1}{2} e^{-\frac{\sigma_z^2}{2}(k+nk_r)^2} \, e^{-\frac{1}{2}k^2(n_x^2+n_y^2)\sigma_{n\perp eff}^2} \right|^2 \right\}, \quad \text{(A11)}$$

where we assume

$$a_n(x,y) = a_{n0} e^{-\alpha_n (x^2+y^2)}, \quad \text{(A12)}$$

and $\sigma_x = \sigma_y = \sigma_\perp$, and

$$\sigma_{n\perp eff} \equiv \frac{\sigma_\perp}{\sqrt{1+2\alpha_n \sigma_\perp^2}}. \quad \text{(A13)}$$

In polar coordinates, the direction cosine reads

$$n_x^2 + n_y^2 = \sin^2\theta_0. \quad \text{(A14)}$$

The single electron radiation spectrum [59, 60] reads, in MKS unit,

$$\frac{d^2 I_0}{d\omega d\Omega} = \frac{Z_0 e_0^2 \gamma^2 N_u^2}{4\pi} \sum_{n=1}^{\infty} G_n(K, \gamma\theta_0, \phi_0) H_n\left(\frac{\omega}{\omega_r}\right), \quad \text{(A15)}$$

where, N_u is the number of undulator period in the radiator. While

$$G_n(K, \gamma\theta_0, \phi_0) = \frac{4n^2}{\left(1+\frac{1}{2}K^2+\gamma^2\theta_0^2\right)^2} \left\{ \left[S_1 \gamma\theta_0 \cos\phi_0 - \left(S_1 + \frac{2}{n} S_2\right) \frac{1+\frac{1}{2}K^2+\gamma^2\theta_0^2}{2\gamma\theta_0\cos\phi_0} \right]^2 + (\gamma\theta_0)^2 S_1^2 \sin^2\phi_0 \right\}, \quad \text{(A16)}$$

with

$$S_1 \equiv \sum_{m=-\infty}^{\infty} J_m(n\xi_z) J_{2m+n}(n\xi_x), \quad \text{(A17)}$$

and

$$S_2 \equiv \sum_{m=-\infty}^{\infty} m J_m(n\xi_z) J_{2m+n}(n\xi_x), \quad \text{(A18)}$$

in which,

$$\xi_z \equiv \frac{K^2}{4\left(1+\frac{1}{2}K^2+\gamma^2\theta_0^2\right)}, \quad \text{(A19)}$$

and

$$\xi_x \equiv \frac{2K\gamma\theta_0\cos\phi_0}{1+\frac{1}{2}K^2+\gamma^2\theta_0^2}. \quad \text{(A20)}$$

As we find from the expression of $G_n(K, \gamma\theta_0, \phi_0)$, on-axis, i.e., when $\theta_0 \to 0$, there is radiation only at odd harmonics.

$$H_n\left(\frac{\omega}{\omega_r}\right) = \frac{\sin^2[N_u \pi(\omega/\omega_r - n)]}{\pi^2 N_u^2 (\omega/\omega_r - n)^2}. \quad \text{(A21)}$$

Up to this point, it is clear that, both the coherent enhancement factor $|F_n|^2$, and the single electron spectrum $\frac{d^2 I_0}{d\omega d\Omega}$ provide the information about the angular distribution, via. θ_0 and ϕ_0, and also the bandwidth. For most cases, the bandwidth at the nth harmonic, is determined by $|F_n|^2$, which has a much narrower bandwidth than does the spontaneous radiation $\frac{d^2 I_0}{d\omega d\Omega}$. We therefore integrate over ω around $\omega_n \equiv n\,\omega_r$ for $|F_n|^2$, while keeping $H_n(\frac{\omega}{\omega_r}) \approx 1$ within this bandwidth. Then we integrate over all the solid angle to get the total energy radiated at the nth harmonic. After so doing, we are left with

$$I_n = \frac{\sigma_{n\perp eff}^4}{\sigma_\perp^4} \frac{Z_0 a_{n0}^2 N_e^2 e_0^2 \gamma^2 N_u^2 c}{16\sqrt{\pi}\sigma_z} \times \int d\Omega G_n(K, \gamma\theta_0, \phi_0) Q_n(\theta_0), \quad \text{(A22)}$$

where

$$Q_n(\theta_0) = \frac{1}{\sqrt{1+\frac{\sigma_{n\perp eff}^2 \sin^2\theta_0}{\sigma_z^2}}} \times \exp\left\{-\frac{n^2\omega_r^2\sigma_z^2}{c^2}\left[1-\frac{1}{1+\frac{\sigma_{n\perp eff}^2\sin^2\theta_0}{\sigma_z^2}}\right]\right\}. \tag{A23}$$

Note that in Eq. (A15), both $\omega = n\,\omega_r$ and $\omega = -n\,\omega_r$ are included already, hence effectively we need only pick up the positive frequency term in Eq. (A11). Completing the integral numerically, we could calculate the radiation energy for any harmonics, odd and even. Suppose the radiator is resonant to the mth harmonic of the seed laser, the Fourier coefficients $a_n = 2\,b_{n\times m}$, and $b_{n\times m}$ is the bunching factor and could be computed according to Eq. (1) in Sec. III B. 1. These Fourier coefficients could also be obtained from TDA code [55]. We compared these two approaches and found good agreements.

From the expression of $Q_n(\theta_0)$ in Eq. (A23), we know, the opening angle

$$\bar{\theta_0} \approx \frac{\lambda_r}{2\pi n\sigma_{n\perp eff}}. \tag{A24}$$

Thus the higher the harmonic, the smaller the opening angle. Also, the larger the e-beam transverse size, the smaller the opening angle.

Equation (A24) could also be obtained by a general consideration of the uncertainty principle, which tells us that the transverse wavevector should satisfy a condition regarding a finite cross section,

$$nk_\perp\sigma_\perp \sim 1, \tag{A25}$$

therefore,

$$k_\perp \sim \frac{1}{n\sigma_\perp}. \tag{A26}$$

Thus the opening angle is just

$$\bar{\theta_0} \sim \frac{k_\perp}{k_\parallel} \approx \frac{k_\perp}{k_r} \approx \frac{1}{k_r n\sigma_\perp}. \tag{A27}$$

This agrees with Eq. (A24).

For the fundamental and also the odd harmonics, the radiation is mainly on-axis, hence, we could make the following approximation.

$$\begin{aligned}
&\int d\Omega G_n(K,\gamma\theta_0,\phi_0)Q_n(\theta_0)\\
\approx\ &\int_0^{2\pi} d\phi_0 \int_0^{\bar{\theta_0}} \sin\theta_0 d\theta_0 G_n(K,\gamma\theta_0,\phi_0)Q_n(\theta_0)\\
\approx\ &G_n(K,\gamma\theta_0,\phi_0)|_{\theta_0=0}Q_n(\theta)|_{\theta_0=0}2\pi(1-\cos\bar{\theta_0})\\
\approx\ &\pi\bar{\theta_0}^2 G_n(K,\gamma\theta_0,\phi_0)|_{\theta_0=0},
\end{aligned} \tag{A28}$$

where we already used the fact that $Q_n(\theta_0)|_{\theta_0=0} = 1$, and $G_n(K,\gamma\theta_0,\phi_0)|_{\theta_0=0}$ is independent of ϕ_0. We also know that in the limit $\theta_0 = 0$,

$$\begin{aligned}
G_n(K,\gamma\theta_0,\phi_0)|_{\theta_0=0} \approx\ &\frac{n^2K^2}{\left(1+\frac{K^2}{2}\right)^2}\\
&\left[J_{\frac{n+1}{2}}\left(\frac{nK^2}{4+2K^2}\right) - J_{\frac{n-1}{2}}\left(\frac{nK^2}{4+2K^2}\right)\right]^2.
\end{aligned} \tag{A29}$$

Thus, for odd harmonics, we would have

$$\begin{aligned}
&\int d\Omega G_n(K,\gamma\theta_0,\phi_0)Q_n(\theta_0) \approx \frac{\pi}{k_r^2\sigma_{n\perp eff}^2}\frac{K^2}{\left(1+\frac{K^2}{2}\right)^2}\\
&\times\ \left[J_{\frac{n+1}{2}}\left(\frac{nK^2}{4+2K^2}\right) - J_{\frac{n-1}{2}}\left(\frac{nK^2}{4+2K^2}\right)\right]^2\\
&\equiv\ \left(\int d\Omega G_n(K,\gamma\theta_0,\phi_0)Q_n(\theta_0)\right)\Bigg|_{approx.}
\end{aligned} \tag{A30}$$

The value of such an approximation is checked with a numerical integral, and good agreement is found.

Once we had computed the radiated energy, we found the peak power of the coherent emission,

$$P_n^{Coh} = \frac{I_n}{\sqrt{2\pi}\sigma_t}, \tag{A31}$$

where, approximately, we have

$$\begin{aligned}
I_n =\ &\frac{\sigma_{n\perp eff}^4}{\sigma_\perp^4}\frac{Z_0 a_{n0}^2 N_e^2 e_0^2\gamma^2 N_u^2 c}{16\sqrt{\pi}\sigma_z}\frac{\pi}{k_r^2\sigma_{n\perp eff}^2}\frac{K^2}{\left(1+\frac{K^2}{2}\right)^2}\\
&\times\ \left[J_{\frac{n+1}{2}}\left(\frac{nK^2}{4+2K^2}\right) - J_{\frac{n-1}{2}}\left(\frac{nK^2}{4+2K^2}\right)\right]^2,
\end{aligned} \tag{A32}$$

hence,

$$\begin{aligned}
&P_n^{Coh}\\
=\ &\frac{\sigma_{n\perp eff}^4}{\sigma_\perp^4}\frac{Z_0 a_{n0}^2 N_e^2 e_0^2\gamma^2 N_u^2}{16\sqrt{2}\sigma_t^2}\frac{1}{k_r^2\sigma_{n\perp eff}^2}\frac{K^2}{\left(1+\frac{K^2}{2}\right)^2}\\
&\times\ \left[J_{\frac{n+1}{2}}\left(\frac{nK^2}{4+2K^2}\right) - J_{\frac{n-1}{2}}\left(\frac{nK^2}{4+2K^2}\right)\right]^2.
\end{aligned} \tag{A33}$$

In most cases, $\sigma_{n\perp eff} \approx \sigma_\perp$, hence we could get a further simplified formula. For the radiation power at the fundamental frequency, we would have,

$$\begin{aligned}
P_1^{Coh} =\ &\frac{Z_0 a_{10}^2 N_e^2 e_0^2\gamma^2 N_u^2}{16\sqrt{2}\sigma_t^2}\frac{1}{k_r^2\sigma_\perp^2}\frac{K^2}{\left(1+\frac{K^2}{2}\right)^2}\\
&\times\ \left[J_1\left(\frac{K^2}{4+2K^2}\right) - J_0\left(\frac{K^2}{4+2K^2}\right)\right]^2.
\end{aligned} \tag{A34}$$

To check the reliability of this analytical approach, we compare our result with the TDA result for the fundamental radiation. Considering that, in TDA, the longitudinal distribution of electron in the pulse is in fact a flat-top model rather than a Gaussian, we should also compute the flat-top model based on this approach.

For a longitudinally flat-top bunch, we have

$$n_0(x,y,z) = \frac{N_e}{2\pi\sigma_x\sigma_y L_z}\, e^{-\frac{x^2}{2\sigma_x^2}}\, e^{-\frac{y^2}{2\sigma_y^2}}, \tag{A35}$$

where, L_z is the length of the bunch.

We repeated the calculation similar to that for the Gaussian model until we got the radiated energy, then the peak power,

$$P_n^{Coh} = \frac{I_n}{L_t}, \tag{A36}$$

where, approximately, we would have

$$I_n = \frac{\sigma_{n\perp eff}^4}{\sigma_\perp^4}\frac{Z_0 a_{n0}^2 N_e^2 e_0^2\gamma^2 N_u^2 c}{8L_z}\frac{\pi}{k_r^2\sigma_{n\perp eff}^2}\frac{K^2}{\left(1+\frac{K^2}{2}\right)^2} \times \left[J_{\frac{n+1}{2}}\left(\frac{nK^2}{4+2K^2}\right) - J_{\frac{n-1}{2}}\left(\frac{nK^2}{4+2K^2}\right)\right]^2, \tag{A37}$$

hence,

$$P_n^{Coh} = \frac{\sigma_{n\perp eff}^4}{\sigma_\perp^4}\frac{Z_0 a_{n0}^2 N_e^2 e_0^2\gamma^2 N_u^2}{8L_t^2}\frac{\pi}{k_r^2\sigma_{n\perp eff}^2}\frac{K^2}{\left(1+\frac{K^2}{2}\right)^2} \times \left[J_{\frac{n+1}{2}}\left(\frac{nK^2}{4+2K^2}\right) - J_{\frac{n-1}{2}}\left(\frac{nK^2}{4+2K^2}\right)\right]^2. \tag{A38}$$

Again, in most cases, $\sigma_{n\perp eff} \approx \sigma_\perp$, hence we could get a further simplified formula. For the radiation power at the fundamental frequency, we would have

$$P_1^{Coh} = \frac{Z_0 a_{10}^2 N_e^2 e_0^2\gamma^2 N_u^2}{8L_t^2}\frac{\pi}{k_r^2\sigma_\perp^2}\frac{K^2}{\left(1+\frac{K^2}{2}\right)^2} \times \left[J_1\left(\frac{K^2}{4+2K^2}\right) - J_0\left(\frac{K^2}{4+2K^2}\right)\right]^2. \tag{A39}$$

If the radiator is resonant to the mth harmonic of the seed laser in the modulator, then by comparing Eq. (A8) with the definition of the bunching factor in Eq. (1) in Sec. III B, we know that $a_n = 2\, b_{n\times m}$, and therefore the above formula could be written as

$$P_1^{peak} = \frac{Z_0\, I_{peak}^2}{8}\frac{1}{4\pi\sigma_x^2}\left(\frac{K\,[JJ]}{\gamma}\right)^2 (b_m\, z)^2, \tag{A40}$$

where $I_{peak} = \frac{N_e\, e_0}{L_t}$.

To do a more precise estimate, then we need to consider the phase advance in the modulator and the radiator as we discussed for Eq. (A10) and (A11). Also, as Eq. (A5) shows, the energy modulation varies transversely, therefore the bunching factor is not a constant across the e-beam. Therefore the $b_m\, z$ term in Eq. (A40) needs to be generalized as

$$\int_0^z \bar{b}_m(z)\, dz, \tag{A41}$$

where

$$\bar{b}_m(z) = \frac{1}{A}\int b_m(r,z)\, d^2r = \frac{1}{A}\int \exp\left[-\frac{1}{2}\left(\frac{\sigma_\gamma}{\Delta\gamma(r)}\right)^2 [\Delta\psi_{mod}(r) + \Delta\psi_{disp}(r) + \Delta\psi_{rad}(r,z)]^2\right] \times J_m\left[\Delta\psi_{mod}(r) + \Delta\psi_{disp}(r) + \Delta\psi_{rad}(r,z)\right] d^2r, \tag{A42}$$

based on Eqs. (1), (A8), (A10) and (A11). A is the transverse beam size. This leads to Eq. (B16) in Sec. III B. 4.1.

APPENDIX B: AMPLIFIED GUIDED MODE

We will use the same notation as in Ref. [6]. We begin from Eq. (5.14) of Ref. [6], but we use the dimensionless variable $x = \sqrt{2\, k_s\, k_w} r$, therefore the total radiation power is

$$P = \frac{1}{Z_0\, 2\, k_s\, k_w}\left\langle \int d^2x |E|^2 \right\rangle. \tag{B1}$$

The field is Fourier transformed as

$$E(\tau,\zeta,\vec{x}) = \frac{1}{2\pi}\int \tilde{E}(\tau, q_\parallel, \vec{x}) e^{iq_\parallel\zeta} dq_\parallel, \tag{B2}$$

where, $\zeta = k_s(z - v_0 t)$. We have

$$\int |E|^2 d\zeta = \frac{1}{2\pi}\int dq_\parallel \left|\tilde{E}(q_\parallel)\right|^2, \tag{B3}$$

hence

$$\left\langle \int |E|^2 d^2x \right\rangle = \frac{1}{2\,\pi\, k_s\, L_z}\int dq_\parallel \int \left|\tilde{E}(q_\parallel)\right|^2 d^2x\,, \tag{B4}$$

where L_z is the e-beam length, and $L_z \to \infty$ is understood. As shown in Eq. (7.23) in Ref. [6], we have

$$E(\tau,\zeta,\vec{x}) = \frac{1}{2\pi i}\sum_n \int d\,q_\parallel \frac{e^{i\,q_\parallel \zeta - i\,\Omega_n(q_\parallel)\tau}}{1-\left(\frac{\partial \Lambda_n}{\partial \Omega}\right)_{\Omega=\Omega_n(q_\parallel)}} \psi\left(\vec{x},q_\parallel\right) S_n\left(q_\parallel\right) \ , \tag{B5}$$

where

$$S_n(q_\parallel) \equiv \int S(\vec{x}',\Omega_n(q_\parallel),q_\parallel)\psi_n(\vec{x}',q_\parallel)d^2x', \tag{B6}$$

and $\psi_n\left(\vec{x},q_\parallel\right)$ is the guided mode. Hence,

$$\tilde{E}\left(\tau,q_\parallel,\vec{x}\right) = \sum_n G_n\left(\tau,q_\parallel\right)\left[-iS_n(q_\parallel)\right]\psi_n\left(\vec{x},q_\parallel\right), \tag{B7}$$

with

$$G_n(\tau,q_\parallel) = \frac{e^{iq_\parallel\zeta - i\Omega_n(q_\parallel)\tau}}{1-\left(\frac{\partial\Lambda_n}{\partial\Omega}\right)_{\Omega=\Omega_n(q_\parallel)}}. \tag{B8}$$

Hence, the power spectrum reads,

$$\frac{dP_{n\,l}}{dq_\parallel} = \frac{1}{2\,k_s\,k_w\,Z_0\,2\,\pi\,k_s} \times \sum_{n,l} G_n\,G_l^*\,\frac{S_n\,S_l^*}{L_z}\int \psi_n\,\psi_l^*\,d^2x\ . \tag{B9}$$

Now, let us focus on the fundamental mode and write

$$\frac{dP_{00}}{dq_\parallel} = \frac{1}{2\,k_s\,k_w\,Z_0\,2\,\pi\,k_s}|G_0|^2\frac{|S_0|^2}{L_z}\int|\psi_0|^2\,d^2x. \tag{B10}$$

For initial bunching, according to Eq. (7.12) of Ref. [6], we have

$$S(\vec{x},\Omega,q_\parallel) = -D_1\int\frac{d\gamma}{\gamma}\frac{\tilde{F}(\tau=0,\vec{x},\gamma,q_\parallel)}{\Omega-\eta(\gamma)(1+q_\parallel)}, \tag{B11}$$

with

$$\begin{aligned}\tilde{F} &= \int_{-\infty}^{\infty} d\zeta e^{-iq_\parallel\zeta}F \\ &= \int_{-\infty}^{\infty} d\zeta e^{-iq_\parallel\zeta}e^{-i\zeta}f(\tau,\zeta,\vec{x},\gamma).\end{aligned} \tag{B12}$$

Let us now assume that the energy spread is small, hence $f \sim \delta(\gamma-\gamma_0)$, and there is a spatial bunching in the electron beam, i.e.

$$\begin{aligned}\int d\gamma f &= 1+\sum a_n\cos n\zeta \\ &= 1+\frac{a_1}{2}e^{i\zeta}+\frac{a_1}{2}e^{-i\zeta}+\cdots\ .\end{aligned} \tag{B13}$$

Therefore,

$$\int d\gamma\tilde{F} = \int_{-\infty}^{\infty} d\zeta e^{-iq_\parallel\zeta}\frac{a_1}{2} = \frac{a_1}{2}2\pi\delta(q_\parallel). \tag{B14}$$

Hence,

$$S_0(q_\parallel) = -\frac{D_1}{\gamma_0}\frac{1}{\Omega-\eta(\gamma_0)(1+q_\parallel)}2\pi\delta(q_\parallel)\int\frac{a_1(\vec{x}')}{2}\psi_0(\vec{x}',q_\parallel)d^2x'\ . \tag{B15}$$

Thus finally we get

$$P_{00} = \int \frac{dP_{00}}{dq_{\|}} dq_{\|} = \frac{1}{2\,k_s\,k_w}\frac{1}{2} m\,c^2\,\gamma_0\,n_0\,(2\rho)^3\,c|\tilde{b}_m|^2 \left|\frac{G_0}{\Omega-\eta(\gamma_0)}\right|^2 \int |\psi_0|^2 d^2x$$
$$= \frac{Z_0 I_{peak}^2}{8}\frac{1}{A}\left(\frac{K[JJ]}{\gamma_0}\right)^2 |\tilde{b}_m|^2 (2\,L_{G\,r})^2 \left\{\frac{1}{2\,k_s\,k_w\,A}\left|\frac{Im\,\lambda}{\lambda}\right|^2 |G_0|^2 \int |\psi_0|^2 d^2x\right\}, \tag{B16}$$

where we have used $L_{G\,r} = \frac{\lambda_w}{8\,\pi\,\rho\,Im\,\lambda}$ is the power e-folding length, and

$$\tilde{b}_m = \int \frac{a_1(\vec{x}')}{2}\psi_0(\vec{x}',0)d^2x' = \int b_m(\vec{x}')\psi_0(\vec{x}',0)d^2x', \tag{B17}$$

in which we again assume the radiator is resonant to the mth harmonic of the seed laser. Arriving the above expression Eq. (B16), we have used the fact that, $\eta(\gamma_0) = 0$. The transverse area is defined as $I_{peak} = e\,n_0\,c\,A$ for a flat-top model, with $A = \pi\,r_0^2$. In the case of a Gaussian distribution as in Appendix A, the area $A = 4\,\pi\,\sigma_\perp^2$. We now work out the details for the flat-top model, which is solved completely in Ref. [6]. In the limit of $\tilde{a} \to \infty$, we have $|\lambda| \to 1$, $|\mathrm{Im}\,\lambda| \to \frac{\sqrt{3}}{2}$, $|G_0|^2 \to \frac{1}{9}e^{\frac{z}{L_{G\,r}}}$, $\int |\psi_0|^2\,d^2x = 1$, and

$$\psi_0(x,0) \to C_0 J_0\left(\mu_{01}\frac{x}{a}\right), \tag{B18}$$

with $\mu_{01} \approx 2.4$, the first root of the Bessel function $J_0(x)$. According to the normalization condition of Eq. (6. 29) of Ref. [6], we know that

$$C_0^2 \to \frac{1}{|J_1(\mu_{01})|^2\,2\,k_s\,k_w\,A}. \tag{B19}$$

Therefore,

$$\tilde{b}_m \approx 2\,k_s\,k_w\,C_0 \int b_m(r)\,J_0\left(\mu_{01}\frac{r}{r_0}\right)d^2r$$
$$= 2\,k_s\,k_w\,A\,C_0\left(\frac{\int b_m(r)\,J_0\left(\mu_{01}\frac{r}{r_0}\right)d^2r}{A}\right)$$
$$= \sqrt{2\,k_s\,k_w\,A}\frac{1}{J_1(\mu_{01})}\bar{b}_m\,R, \tag{B20}$$

with

$$R = \frac{\frac{1}{A}\int b_m(r)\,J_0\left(\mu_{01}\frac{r}{r_0}\right)d^2r}{\bar{b}_m} \tag{B21}$$

Thus we have

$$P_{00} = \frac{Z_0 I_{peak}^2}{8}\frac{1}{A}\left(\frac{K[JJ]}{\gamma_0}\right)^2 |\bar{b}_m|^2 (2\,L_{G\,r})^2 \frac{1}{12}\,e^{\frac{z}{L_{G\,r}}}\frac{R^2}{|J_1(\mu_{01})|^2} \equiv C_{00}\,P_1^{coh}(z = 2\,L_{G\,r})\,e^{\frac{z}{L_{G\,r}}}, \tag{B22}$$

where $|\bar{b}_m|^2(2\,L_{G\,r})^2$ is generalized to be

$$\left(\int_0^{2\,L_{G\,r}} \bar{b}_m(z)\,dz\right)^2, \tag{B23}$$

considering the transverse and also longitudinal variation of the bunching factor, and

$$C_{00} = \frac{1}{12}\frac{R^2}{|J_1(\mu_{01})|^2}. \tag{B24}$$

We know from Eq. (1) that the bunching factor $b_m(r) \propto J_m\left(\alpha e^{-r^2/\bar{w}^2}\right)$, with α a constant. Since $\psi_0(\vec{r},0) \propto J_0\left(\mu_{01}\frac{r}{r_0}\right)$ from the above Eq. (B18), the width of the bunching factor is much narrower than that of the guided mode $\psi_0(\vec{r},0)$. Hence we could move $J_0\left(\mu_{01}\frac{r}{r_0}\right)$ out of the integral in R of Eq. (B21), and therefore

$$R \approx \frac{J_0\left(\mu_{01}\frac{r^{ap}}{r_0}\right)\frac{1}{A}\int b_m(r)d^2r}{\bar{b}_m} = J_0\left(\mu_{01}\frac{r^{ap}}{r_0}\right). \tag{B25}$$

Thus, if we choose $r^{ap} = 0$, then $R = 1$, and therefore

$$C_{00} = \frac{1}{12}\frac{1}{|J_1(\mu_{01})|^2} \approx \frac{3.71}{12} \approx \frac{1}{3}. \tag{B26}$$

Since $R = 1$ is obviously an overestimation, if we choose $r^{ap} = \frac{\sigma_\perp}{\sqrt{2}}$, then for a matched beam, i.e., $\bar{w} = \sqrt{2}\sigma_\perp = \frac{r_0}{\sqrt{2}}$, we have $R = J_0\left(\frac{\mu_{01}}{2\sqrt{2}}\right)$, and therefore

$$C_{00} = \frac{1}{12}\left|\frac{J_0\left(\frac{\mu_{01}}{2\sqrt{2}}\right)}{J_1(\mu_{01})}\right|^2 \approx \frac{1}{5}. \tag{B27}$$

For a general case of $\tilde{a}$, we need use a software as Mathematica [61] to solve a few equations. This could be done similar to what was done for the SASE case [10].

[1] Ya.S. Derbenev, A.M. Kondratenko, and E.L. Saldin, *Nucl. Instrum. Methods Phys. Res. A* **193**, 415(1982).
[2] R. Bonifacio, C. Pellegrini, and L.M. Narducci, *Opt. Commun.* **50**, 373(1984).
[3] J.M. Wang, and L.H. Yu, *Nucl. Instrum. Methods Phys. Res. A* **250**, 484(1986).
[4] K.J. Kim, *Nucl. Instrum. Methods Phys. Res. A* **250**, 396(1986).
[5] K.J. Kim, *Phys. Rev. Lett.* **57**, 1871(1986).
[6] S. Krinsky, and L.H. Yu, *Phys. Rev. A* **35**, 3406(1987).
[7] L.H. Yu, S. Krinsky, and R.L. Gluckstern, *Phys. Rev. Lett.* **64**, 3011(1990).
[8] L.H. Yu, S. Krinsky, R.L. Gluckstern, and J.B.J. van Zeijts, *Phys. Rev. A* **45**, 1163(1992).
[9] R. Bonifacio, L. De Salvo, P. Pierini, N. Piovella, and C. Pellegrini, *Phys. Rev. Lett.* **73**, 70(1994).
[10] Li Hua Yu, *Phys. Rev. E* **58**, 4991(1998).
[11] S. Krinsky, *Phys. Rev. E* **59**, 1171(1999).
[12] B.W.J. McNeil, G.R.M. Robb, D.A. Jaroszynski, *Opt. Comm.* **165**, 65(1999).
[13] M.J. Hogan, *et al. Phys. Rev. Lett.* **82**, 4867(1998).
[14] S.V. Milton, *et al.*, *Phys. Rev. Lett.* **85**, 988(2000); S.V. Milton, *et al.*, *Science*, **292**, 2037(2001).
[15] J. Andruszkow, *et al.*, *Phys. Rev. Lett.* **85**, 3825(2000); V. Ayvazya, *et al.*, *Phys. Rev. Lett.* **88**, 104802(2002).
[16] L.H. Yu, *Phys. Rev. A* **44**, 5178(1991).
[17] I. Ben-Zvi, L.F. Di Mauro, S. Krinsky, M.G. White, and L.H. Yu, *Nucl. Instrum. Methods Phys. Res. A* **304**, 151(1991).
[18] I. Ben-Zvi, A. Friedman, C.M. Hung, G. Ingold, S. Krinsky, and L.H. Yu, *Nucl. Instrum. Methods Phys. Res. A* **318**, 208(1992).
[19] L.-H. Yu, *et al.*, *Nucl. Instrum. Methods Phys. Res. A*, **445**, 301(2000).
[20] L.-H. Yu, *et al.*, *Science*, **289**, 932(2000).
[21] Li Hua Yu and Juhao Wu, *Nucl. Instrum. Methods Phys. Res. A*, **483**, 493(2002).
[22] A. Doyuran, *et al.*, *Phys. Rev. Lett.* **86**, 5902(2001)
[23] L.H. Yu, *et al.*, *Phys. Rev. Lett.* **91**, 074801(2004)
[24] A. Doyuran, *et al.*, *Phys. Rev. ST Accel. Beams* **7**, 050701(2004).
[25] N.A. Vinokurov, and A.N. Skrinsky, preprint INP 77-59, Novosibirsk (1977).
[26] P. Czonka, *Part. Accel.* **8**, 225(1978).
[27] V. Stagno, G. Brautti, T. Clauser, and I. Boscolo, *Nuovo Cimento B* **56**, 219 (1980)
[28] I. Boscolo and V. Stagno, *Nuovo Cimento B* **56**, 219(1980).
[29] W.B. Colson, *IEEE J. Quant. Electron.* **QE-17**, 1417(1981).
[30] R. Coïsson, and F. DeMartini, in *Physics of Quantum Electronics* Vol. 9, Eds. S.F. Jacobs, M. Sargent III, and M.O. Scully, P. 939, Addison-Wesley, Reading, MA, (1982).
[31] I. Boscolo, and V. Stagno, *Nucl. Instrum. Methods Phys. Res. A* **198**, 483 (1982).
[32] W.B. Colson, and P. Elleaume, *Appl. Phys. B* **29**, 101 (1982).
[33] I. Schnitzer, and A. Gover, *Nucl. Inctrum. Methods Phys. Res. A* **237**, 124 (1985).
[34] R. Bonifacio, L. De Salvo Souza, P. Pierini, and E.T. Scharlemann, *Nucl. Instrum. Methods Phys. Res. A* **296**, 787 (1990).
[35] R. Prazeres, P. Guyot-Sionnest, J.M. Ortega, D. Jaroszynski, M. Billardon, M.E. Couprie, M. Velghe, and Y. Petroff, *Nucl. Instrum. Methods Phys. Res. A* **304**, 72 (1991).
[36] R. Bonifacio, R. Corsini, and P. Pierini, *Phys. Rev. A* **45**, 4091 (1992).
[37] D.A. Jaroszynski, R. Prazers, F. Glotin, O. Marcouille, J.M. Ortega, *Nucl. Instrum. Methods Phys. Res. A* **375**, 456 (1996).
[38] E.L. Saldin, E.A. Schneidmiller, and M.V. Yurkov, *Nucl. Instrum. Methods Phys. Res. A* **381**, 545(1996)
[39] L.H. Yu, *Proceedings of the IFCA Advanced Beam Dynamics Workshop on Future Light Sources*, C.E. Eyberger, Ed., Argonne National Laboratory, Argonne, IL(1999) (URL: http: //www.aps.anl.gov /conferences /FLSworkshop /proceedings /papers /wg1-01.pdf).).
[40] Juhao Wu, and Li Hua Yu, *Nucl. Instrum. Methods Phys. Res. A*, **475**, 104(2001).
[41] L.H. Yu, and Ilan Ben-Zvi, *Nucl. Instrum. Methods Phys. Res. A*, **393**, 96(1997).
[42] G. Dattoli, and P.L. Ottaviani, *J. Appl. Phys.*, **86**, 5331(1999).
[43] Juhao Wu, and Li Hua Yu, SLAC Report No. SLAC-PUB-10495, 2004.
[44] I. Ben-Zvi, K.M. Yang, and L.H. Yu, *Nucl. Instrum. Methods Phys. Res. A* **318**, 726(1992).
[45] E.L. Saldin, E.A. Schneidmiller, and M.V. Yurkov, *Opt. Commun.* **202**, 169(2002).
[46] Juhao Wu, *Proceedings of the 2003 Particle Accelerator Conference*, Portland, Oregon, U.S.A., May 12 - 16, 2003, Editors: J. Chew, P. Lucas, and S. Webber, P. 1035.
[47] A. Yariv, *Quantum Electronics*, John Wiley and Sons, New York, (1975).
[48] G.T. Moore, *Nucl. Instrum. Methods Phys. Res. A*, **239**, 19(1985).
[49] E.T. Scharlemann, A.M. Sessler and J.S. Wurtele, *Phys. Rev. Lett.* **54**, 1925(1985).
[50] L.-H. Yu and S. Krinsky, *Nucl. Instrum. Methods Phys. Res. A*, **285**, 119(1989).
[51] Juhao Wu, and Li Hua Yu, *Nucl. Instrum. Methods Phys. Res. A*, **475**, 79(2001).
[52] M. Xie, *IEEE Proceedings for Pac95*, P. 183, (1995).
[53] K.J. Kim, and M. Xie, *Nucl. Instrum. Methods Phys. Res. A* **331**, 359(1993).
[54] "Linac Coherent Light Source (LCLS) Design Study Report," The LCLS Design Study Group, Standford Linear Accelerator Center (SLAC) Report No. SLAC-R-521(1998).
[55] T.M. Tran, and J.S. Wurtele, *Comput. Phys. Commun.* **54**, 263(1989).
[56] Z. Huang, and K.J. Kim, *Phys. Rev. E* **62**, 7295(2000).

[57] J.D. Jackson, *Classical Electrodynamics* Eq. (14.67), John Wiley and Sons, New York, (1965).

[58] B.M. Kincaid, R.R. Freeman, C. Pellegrini, A. Luccio, S. Krinsky, A. van Steenbergen, and F. Demartini, in *Free Electron Generation of Extreme Ultraviolet Coherent Radiation*, Eds. J.M.J. Madey and C. Pellegrini, AIP Conference Proceedings, No. 118, P. 110(1984); B.M. Kincaid, and R.R. Freeman (unpublished).

[59] S. Krinsky, M.L. Perlman, and R.E. Watson, in *Handbook on Synchrotron Radiation, Vol. 1*, Eds. E.E. Koch, P. 65, North-Holland Publishing Company, (1983).

[60] D.F. Alferov, Yu.A. Bashmakov, and E.G. Bessonov, *Sov. Phys. Tech. Phys.* **18**, 1336(1974).

[61] *Mathematica*, Wolfram Research, Inc.